Seismic Slope Stability: A Comparison Study of Empirical Predictive Methods with the Finite Element Method

by

Julio Copana

Thesis submitted to the faculty of the
Virginia Polytechnic Institute and State University
in partial fulfillment of the requirements for the degree of

Master of Science
In
Civil Engineering

Alba Yerro-Colom, Chair
Adrian Rodriguez-Marek
Matthew Mauldon

September 30th, 2020
Blacksburg, Virginia

Keywords: Slope stability, earthquake, finite element method, ground motion prediction equation

Seismic Slope Stability: A Comparison Study of Empirical Predictive Methods with the Finite Element Method

Julio Copana

ABSTRACT

This study evaluates the seismically induced displacements of a slope using the Finite Element Method (FEM) in comparison to the results of twelve empirical predictive approaches. First, the existing methods to analyze the stability of slopes subjected to seismic loads are presented and their capabilities to predict the onset of failure and post-failure behavior are discussed. These methods include the pseudostatic method, the Newmark method, and stress-deformation numerical methods. Whereas the pseudostatic method defines a seismic coefficient for the analysis and provides a safety factor, the Newmark method incorporates a yield coefficient and the actual acceleration time history to estimate permanent displacements. Numerical methods incorporate advanced constitutive models to simulate the coupled stress-strain soil behavior, making the process computationally more costly. In this study, a model slope previously studied at laboratory scale is selected and scaled up to prototype dimensions. Then, the slope is subjected to 88 different input motions, and the seismic displacements obtained from the numerical and empirical approaches are compared statistically. From correlation analyses between seven ground motion parameters and the numerical results, new empirical predictive equations are developed for slope displacements. The results show that overall the FEM displacements are generally in agreement with the numerically developed methods by Fotopoulou and Pitilakis (2015) labelled "Method 2" and "Method 3", and the Newmark-type Makdisi and Seed (1978) and Bray and Travasarou (2007) methods for rigid slopes. Finally, functional forms for seismic slope displacement are proposed as a function of peak ground acceleration (PGA), Arias intensity (I_a), and yield acceleration ratio (A_y/PGA). These functions are expected to be valid for granular slopes such as earth dams, embankments, or landfills built on a rigid base and with low fundamental periods (T_s<0.2).

Seismic Slope Stability: A Comparison Study of Empirical Predictive Methods with the Finite Element Method

Julio Copana

GENERAL AUDIENCE ABSTRACT

A landslide is a displacement on a sloped ground that can be triggered by earthquake shaking. Several authors have investigated the failure mechanisms that lead to landslide initiation and subsequent mass displacement and proposed methodologies to assess the stability of slopes subjected to seismic loads. The development of these methodologies has to rely on field data that in most of the cases are difficult to obtain because identifying the location of future earthquakes involves too many uncertainties to justify investments in field instrumentation (Kutter, 1995). Nevertheless, the use of scale models and numerical techniques have helped in the investigation of these geotechnical hazards and has led to development of equations that predict seismic displacements as function of different ground motion parameters. In this study, the capabilities and limitations of the most recognized approaches to assess seismic slope stability are reviewed and explained. In addition, a previous shaking-table model is used for reference and scaled up to realistic proportions to calculate its seismic displacement using different methods, including a Finite Element model in the commercial software Plaxis2D. These displacements are compared statistically and used to develop new predictive equations. This study is relevant to understand the capabilities of newer numerical approaches in comparison to classical empirical methods.

ACKNOWLEDGMENT

I would like to recognize to all the individuals who have assisted me in different ways during my master's degree. First, I want to express my deep gratitude to my advisors, Prof. Alba Yerro-Colom and Prof. Adrian Rodriguez-Marek for their continuous support throughout my degree completion. Their knowledge, motivation, guidance, and encouragement to complete this research are greatly appreciated.

Also, I am thankful to Prof. Matthew Mauldon for being part of my committee members and providing advice. Special thanks to the PhD students Luis Zambrano and Mahdi Bahrampouri for their help and feedback in various topics of this research.

I extend my gratitude to the faculty in the geotechnical engineering program for fostering excellent professionals and being part of my educational training. I am also thankful to the Geotechnical Student Organization for providing unique opportunities to interact among graduate students and to make my journey in Blacksburg very memorable. Similarly, I offer my appreciation to the Fulbright Program for the opportunity to further continue my education.

Finally, I want to thank to my parents and brother for supporting my dreams since early stages of my life, and to my friends in Bolivia for their care especially during this particular year.

TABLE OF CONTENTS

Chapter 1. Introduction **1**

1.1. Motivation 1
1.2. Research objectives 2
1.3. Organization 2

Chapter 2. Methods to Assess Seismic Slope Stability **3**

2.1. Introduction 3
2.2. Pseudostatic analysis 4
2.3. Sliding block analysis 6
2.4. Stress deformation analysis 8
2.5. Conclusion 10

Chapter 3. Seismic Slope Stability: A Comparison Study of Empirical Predictive Methods with the Finite Element Method **12**

3.1. Introduction 12
3.2. Methodology 13
3.2.1. Prototype and scale model characteristics 13
3.2.2. Dynamic resistance and rigidity of the slope 15
3.2.3. Earthquake ground motions 15
3.2.4. Empirical predictive methods 16
3.2.5. Finite element model 23
3.3. Results 25

Chapter 4. Discussion **28**

4.1. Direct comparison 28
4.2. Statistical measures 30
4.3. Scoring procedure 34
4.4. Empirical predictive equations based on the finite element method (FEM) 35
4.5. Effects of FEM mesh size on the predictive equations 40

Chapter 5. Conclusions **42**

5.1. Future work 44

References **45**

Appendix

Appendix A. Seismic records used for the numerical and empirical analysis 48

Appendix B. Histograms of Intensity Measures 50

Appendix C. Correlations between ground motion parameters 51

Appendix D. Summary of seismic displacements and ground motion parameters 52

Appendix E. Histograms of seismic displacements obtained from the empirical and numerical methods 54

Appendix F. Fitted functions with empirical data points 57

LIST OF TABLES

Table 1.	Summary of the applicability of the methods on a) stability and b) post-failure analysis	11
Table 2.	Empirical Predictive Equations for Seismic Slope Stability	22
Table 3.	Material properties	24
Table 4.	Maximum permanent displacements calculated from empirical approaches along with the corresponding displacement obtained with FEM for the same ground motion record	25
Table 5.	Summary of statistical errors between numerical and empirical methods	31
Table 6.	Summary of scored statistical measures	34
Table 7.	Regression coefficients for estimating the probability of non-zero displacements given a certain intensity measure	36
Table 8.	Regression coefficients for estimating the non-zero displacements given a certain intensity measure. Scalar form	37
Table 9.	Regression coefficients for estimating nonzero displacements. Vectorial form	37
Table 10.	Expected displacements for different fundamental periods and dynamic strength	39
Table 11.	Displacements for initial and finer mesh	41
Table 12.	Absolute difference between initial and finer mesh fit measures	41

LIST OF FIGURES

Figure 1.	Free diagram body for an infinite slope with Seismic load kW (From Duncan et al., 2014)	5
Figure 2.	Integration of effective acceleration time-history to determine velocities and displacement	6
Figure 3.	Simplified estimates of the yield coefficient: a) shallow sliding, and b) deep sliding. (From Bray, 2007)	7
Figure 4.	Stress-strain relationships. (a): Elastic perfectly plastic, (b): Elastic-linear hardening, (c): Elastic-linear softening	9
Figure 5.	Flowchart of methodology	14
Figure 6.	Factor of safety vs. seismic coefficient	15
Figure 7.	(a) Fourier Amplitude Spectra, and (b) Response Spectral Acceleration	16
Figure 8.	Acceleration time records and yield acceleration used in the study	17
Figure 9.	(a): Variation of maximum acceleration ratio with depth of sliding mass. (b): Variation of permanent displacement with respect to yield acceleration over MHEA (Makdisi and Seed, 1978)	19
Figure 10.	(a) Initial effective vertical stresses, and (b) prescribed line displacement on mesh	24
Figure 11.	Deformed mesh after FEM dynamic phase subjected to input record N° 28	26
Figure 12.	Numerical horizontal displacement versus time for different records	26
Figure 13.	Cumulative frequency versus permanent displacement	27
Figure 14.	Empirical versus numerical seismic displacements	29
Figure 15.	Cumulative distribution of the relative difference between empirically and numerically calculated seismic displacements	31

Figure 16. Statistical measures for the empirical predictive approaches. (a) RMSE, (b) SMAPE, (c) MRAE, and (d) MASE 32

Figure 17. Averaged score of statistical measures for the empirical predictive approaches 35

Figure 18. Probit regression for (a) PGA, (b) Arias intensity, and (c) A_y/PGA for the probability to obtain 'displacements greater than 0' (0.1 cm) 36

Figure 19. Regression of the horizontal seismic displacements versus intensity measures and their corresponding residuals ($\log D_{data} - \log D_{predicted}$) for: (a) PGA, (b) I_a, (c) A_y/PGA 38

Figure 20. Seismic horizontal displacements versus intensity measures for: (a) PGV, (b) PGD, (c) $D_{5\text{-}95}$, and (d) T_m 39

Figure 21. Log of displacement versus intensity measures. Data of finer mesh plotted on initial fitted line. (a) PGA, (b) Arias intensity, and (c) A_y/PGA 40

CHAPTER 1. INTRODUCTION

1.1. Motivation

A landslide is a geotechnical hazard that can be triggered by different phenomena, and every year causes enormous economic and human losses around the world. The United States Geological Survey (USGS) classifies the triggering mechanisms into two main categories: human and natural. Natural mechanisms combine the effects of water, volcanic activity, and seismic activity. From these triggers, seismic activity has proven to have a great impact on the stability of slopes. For instance, the M 7.5 Guatemala Earthquake in 1976 caused approximately 50,000 landslides (Harp et al., 1981), and the Niigata Ken Chuetsu earthquake in 2004 recounted around 30 landslides/km^2 in a 30-km^2 study area and caused damages estimated at U.S. $8 billion (Kieffer et al., 2006). For that reason, co-seismic landslides have been studied to develop methodologies to assess them and reduce their negative effects.

An important factor for the risk assessment is to predict seismic displacements, which is possible by applying empirical predictive methods or stress-strain numerical methods. The development of predictive equations is a demanding procedure that requires the application of large amounts of data for different configurations. Nevertheless, identifying where earthquakes are going to happen is uncertain, and this restricts engineers from knowing where to invest in field instrumentation to study seismic effects (Kutter, 1995). Therefore, the use of laboratory scale models is important for data acquisition to apply them in geotechnical modeling. In this investigation, a slope model tested on a shaking table is analyzed and used for developing empirical equations.

In addition, even though numerical analyses have better capability to represent the complex dynamic response in comparison to the empirical methods, their historical drawback is the computation time. Nevertheless, the advent of newer computational tools has increasingly been available to perform dynamic numerical analysis of slopes more efficiently (e.g. Plaxis, FLAC). Therefore, comparison studies of existing empirical methods with newer numerical methods are important to observe the consistency of the results.

1.2. Research Objectives

The aims of the research presented herein are:

- To review the different approaches to evaluate seismic slope stability and identify how these methodologies evaluate the onset of failure and the post-failure analysis of slopes. This will provide insights into the capabilities and limitations of the methods for their correct application.
- To perform a statistical comparison of the seismic displacements obtained from a finite element (FE) numerical model with the permanent displacements of twelve empirical predictive approaches. In particular, we focus on the stability of homogeneous granular slopes such as earth dams, embankments, or landfills built on a rigid base and low fundamental periods. For this purpose, a previous study of a small granular slope on a shaking table experiment is considered and scaled up by a factor of 10. The empirical methods include the approaches developed by Newmark (1965), Makdisi and Seed (1978), Hynes-Griffin and Franklin (1984), Bray and Travasarou (2007), Jibson (2007), Hsieh and Lee (2011), and Fotopoulou and Pitilakis (2015). The FEM numerical model is implemented in the Plaxis2D program.
- To propose new empirical predictive equations for seismically induced granular slopes settled on a rigid base. In this respect, seven ground motion parameters (PGA, PGV, PGD, I_a, T_m, $D_{5\text{-}95}$, A_y/PGA) are correlated to the horizontal displacements obtained from the FE model to fit the best functional forms.

1.3. Organization

This investigation is organized in the following chapters. Chapter 2 describes and classifies the existing methods to assess seismic slope stability and runout. Chapter 3 explains the general methodology used in this research, describes all the empirical predictive approaches used in this study, details the numerical modeling in Plaxis, and presents the results. Chapter 4 discusses the results of the statistical comparison, presents the correlation analyses for the development of predictive equations, and discusses the effect of the FE mesh size in the results. Chapter 5 provides the concluding remarks. Finally, the Appendix presents a tabulated summary of the ground motion parameters, seismic displacements, and additional graphs.

CHAPTER 2. METHODS TO ASSESS SEISMIC SLOPE STABILITY

2.1. Introduction

Seismic slope stability is a geotechnical hazard, and a subject developed through a comprehensive study of landslides triggered by earthquakes. Reports of these events date back to 1789 BCE in China and 373 or 372 BCE in Greece (Hansen and Franks, 1991 and Seed 1968; Keefer, 2002), and the first extensive investigation of landslides triggered by earthquakes was performed in Italy in 1783 (Keefer, 2002). Since then, different authors have not only developed techniques that allow engineers to reduce the uncertainty of sloped earthworks designed for seismic events, but also performed many investigations to improve previous techniques. The understanding of failure mechanisms of sloped materials and the introduction of limit equilibrium methods for its stability analysis brought about by well-known authors in soil mechanics, and simultaneously, the increasing understanding of earthquake waves and its representation were fundamental to advance into the development of the pseudostatic method for seismic slope stability analysis. Later, the seismic displacements as a measure of performance of the slope were introduced. Currently, numerical techniques and advanced computational tools play an important role in the assessment of seismic slope stability analysis. This chapter will summarize the state of the art of the methods used for this purpose.

To begin, Terzaghi (1950) defines a landslide as a rapid displacement of the ground followed by an imperceptible movement called ‘creep’ that occurs when the resistance of the soil is surpassed by the driving forces. A broader definition is given by the USGS which describes it as the downward and outward movement of slope materials and classifies the types of movements into falls, topples, slides, lateral spreads, and flows depending on the direction of the movement, the shape of the failure mechanism, the rate of movement, and the content of other materials such as water, ice or air. In particular, this investigation (Chapter 3) focuses on ‘slides’ type of movements. According to Duncan et al. (2014), a slope failure occurs when the shear strength of the soil required for equilibrium is less than the shear stress. This condition of instability can be achieved by external or internal phenomena. External phenomena are referred to as those that increase the shearing stresses and can be understood as external loads such as seismic loads or induced man-made loads. Internal causes happen when there is a reduction in the shear strength of the soil.

Terzaghi (1950) attributed this loss of strength to the increase of pore pressures and the progressive decrease of the cohesion as the two most common reasons. When an earthquake happens, the increase of the shearing stresses, and a reduction of the shear strength of the soil could occur simultaneously. Therefore, the challenges of seismic slope stability lay on estimating the potential failure surface, the shear strength of the soil along these surfaces, and how to efficiently consider the effects of the seismic loading. Moreover, the challenges of post-failure analysis include the runout prediction.

Several approaches have been studied to include dynamic loads in slope stability analyses. Jibson (2010) describes and classifies the methods that have been developed during the twentieth century in three types: the earliest is the pseudostatic method established by Terzaghi in 1950; then, the estimation of permanent displacement as a mean to analyze the slope stability analysis was introduced by Newmark in 1965; and finally, the use of the finite element method and other numerical techniques gave place to the so-called stress-deformation analysis which can allow for complex constitutive models to represent the dynamic behavior of the slope, and theoretically are the most accurate. The following lines will review and describe these methods emphasizing the seismic evaluation and their applicability for post-failure analyses.

2.2. Pseudostatic Analysis

The pseudostatic method is the earliest approach to assess seismic slope stability. Introduced by Terzaghi in 1950, he describes the use of a coefficient (n_g) defined as the quotient of the greatest horizontal acceleration produced by an earthquake and the gravity acceleration. This coefficient is nowadays denoted as a seismic coefficient (k), and it is the most important parameter of the pseudostatic analysis of slopes. This method incorporates the complex dynamic load as a single unidirectional static force equal to the product of the weight of the sliding mass and the seismic coefficient. The location of the application of the force is not well defined. Terzaghi suggested that it should be applied at the center of gravity of the slices (Duncan et al., 2014). After the application of this pseudostatic horizontal force, a traditional static slope stability analysis is performed using limit equilibrium methods to calculate a factor of safety. For example, Figure 1 presents the configuration of an infinite slope where β is the inclination angle, W is the weight of the slice, and its factor of safety can be computed using Equation 1.

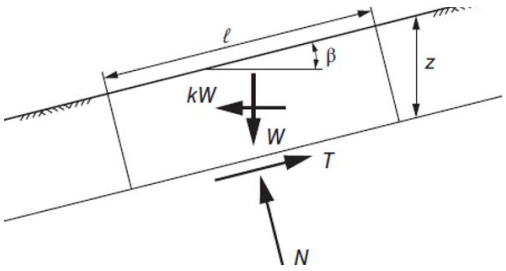

Figure 1. Free diagram body for an infinite slope with seismic load kW (From Duncan et al., 2014)

$$FS = \frac{c + (\gamma z \cos^2\beta - k\gamma z \cos\beta \sin\beta)\tan\phi}{\gamma z \cos\beta \sin\beta + k\gamma z \cos^2\beta} \qquad (1)$$

Several recommendations and expressions are available in the literature to determine the seismic coefficient (k) which generally ranges from 0.05 to 0.25 (Duncan et al., 2014). Hynes-Griffin and Franklin (1984) recommend using a seismic coefficient equal to half of the peak ground acceleration (PGA). Terzaghi (1950) proposed to use 0.1, 0.25, and 0.5 for "severe", "violent", and "catastrophic" events respectively. Melo and Sharma (2004) performed a numerical analysis in FLAC to back-calculate seismic coefficients from real cases; their results ranged from 0.172 to 0.677. Bray and Travasarou (2009) provide a general procedure for selecting the seismic coefficient based on allowable seismic displacements. Their expression (Equation 2) presents k as a function of the parameters a and b, where a is a function of the 5% spectral acceleration (S_a), and b is a function of the seismic displacement (D_a) to be defined by the engineer, the initial fundamental period of the sliding block (T_s), the moment magnitude of the earthquake (M), and the normally distributed random variable (ε). Thus, an accurate estimation of the seismic coefficient is complex, and it requires a lot of engineering judgment.

$$k = \exp\left[\frac{-a + \sqrt{b}}{0.665}\right] \qquad (2)$$

$$a = 2.83 - 0.566\ln(S_a) \qquad (3)$$

$$b = a^2 - 1.33\left[\ln(D_a) + 1.10 - 3.04\ln(S_a) + 0.244\left(\ln(S_a)\right)^2 - 1.5T_s - 0.278(M - 7) - \varepsilon\right] \qquad (4)$$

For periods T_s<0.05 s the term 1.10 in the Equation 4 must be changed to 0.22.

The advantage of the pseudostatic method is that the implementation of a seismic load in the slope stability analysis is straightforward. However, this simplification of a complex load causes the method to be over-conservative. In addition, the typical limitations of limit equilibrium methods are kept in this analysis. For example, the assumption of the location and shape of failure surfaces with an unvarying shear strength all across the surface (resembling uniform plastification). Finally, another drawback of this technique is the lack of information for the post-failure analysis since the serviceability evaluation of a structure after an earthquake is based on displacements (Kramer, 2007).

2.3. Sliding Block Analysis

A factor of safety does not provide any information about the performance of the slope. Therefore, Newmark (1965) introduced the rigid-block analysis to calculate seismically induced permanent displacements on embankments and dams. This approach considers the sliding mass as a rigid body on an inclined surface, and the ground motion is incorporated as an acceleration time-history. The yield acceleration (A_y) is defined as the product of the gravity acceleration and the yield coefficient (k_y). The last term is equivalent to the seismic coefficient (k) that produces a factor of safety equal to one. When the acceleration a(t) exceeds A_y, the block begins to slide, and it stops when the velocity of the block and the velocity of the underlying mass are the same. The accelerations surpassing A_y are integrated once to find the velocity of the system and twice to find a permanent displacement.

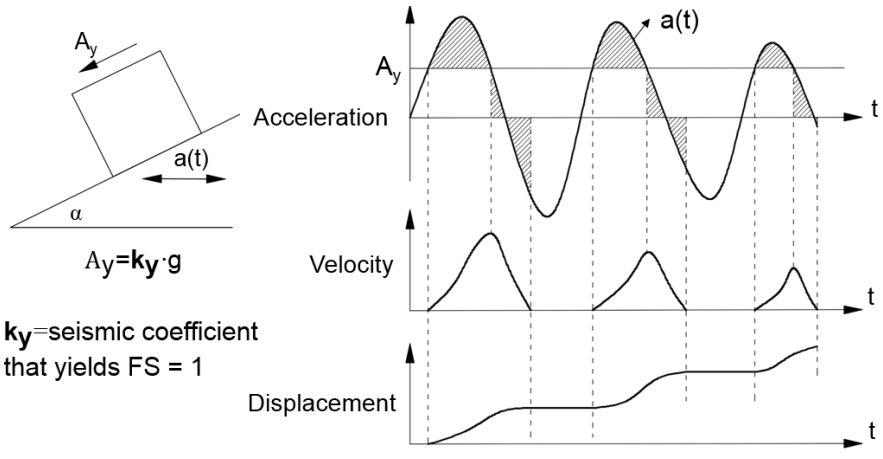

Figure 2**.** Integration of effective acceleration time-history to determine velocities and displacement

The yield coefficient (k_y) is the representation of the dynamic resistance of the slope because it is a function of the material's shear properties (friction angle and cohesion), the geometry of the slope (e.g., height, inclination), and the weight (Bray, 2007). To find k_y, three slip surfaces must be analyzed: i) the slip surface that produces the minimum static factor of safety, ii) the slip surface that produces the minimum k_y, which sometimes could be unrealistic and provide very low k_y values and iii) the slip surface that reflects the pattern of accelerations within the soil mass (Duncan et al., 2014). The lower the k_y value would represent a weaker soil, and conversely, the greater this value, the stronger the soil (Fotopoulou and Pitilakis, 2015)

Jibson (2010) calls the yield acceleration A_y critical acceleration A_c and presents Equation 5 to calculate it as a function of the static factor of safety (FS) and the angle of the slope (α) with the horizontal line. Bray (2007) presents simplified equations to determine k_y as a function of the slope geometry, weight, and strength (see Figure 3).

$$A_c = A_y = (FS - 1)g\sin\alpha \qquad (5)$$

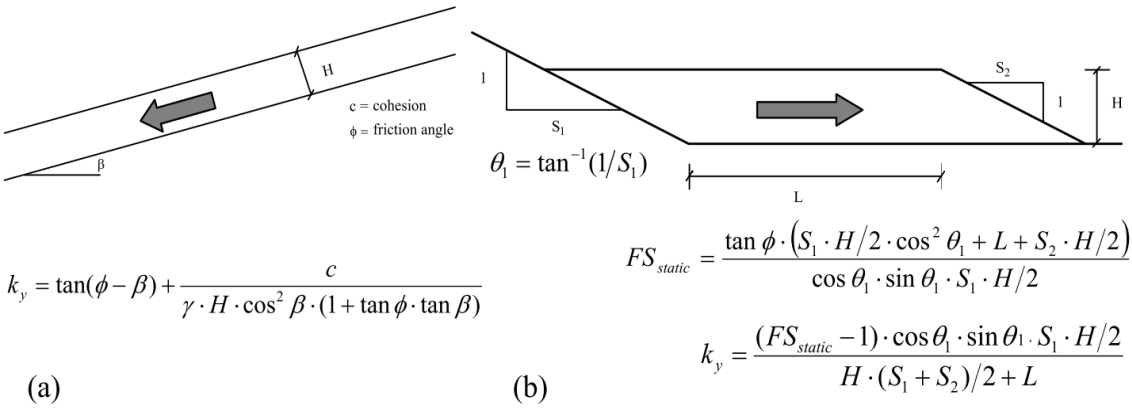

Figure 3. Simplified estimates of the yield coefficient: a) shallow sliding, and b) deep sliding. (From Bray, 2007)

Sliding-block methods can generally be applied to predict displacements resulting from 'slides' type of movements which include rotational and translational landslides (Jibson, 1993). The parameter analyzed to evaluate the performance and determine if the slope will be stable is the allowable permanent displacement. If the final displacement is greater than the allowable permanent displacement, there is a potential risk of failure of the slope. Therefore, several

empirical predictive approaches have been developed using the Newmark approach to calculate permanent displacements as a function of different intensity measures (IM). Lately, risk analyses have been incorporated in the assessment of slopes under seismic loads (Finn, 2013), providing a more comprehensive seismic analysis and where the engineering judgment plays a crucial role in determining allowable permanent displacements. Similarly, values of maximum permanent displacements or threshold displacements (Bray, 2007) have been suggested. In general, allowable deformations generally vary from 0.15 m to 1.0 m (Duncan et al., 2014). Results within these ranges could be subject to posterior risk analysis. In addition, displacements greater than the referential allowable displacements could be categorized as 'large deformations'.

Makdisi and Seed (1978) observed that the peak acceleration on the base is not constant through the slope; instead, there is an amplification of the accelerations from the base to the crest. Rigid block analyses hypothesize that the whole sliding mass is subjected to the exact same motion and they do not accurately capture the dynamic response of the slope during earthquake shaking. To overcome this limitation, Makdisi and Seed (1978) developed charts to estimate permanent Newmark displacements considering the amplification using finite element analyses. The development of similar studies (e.g., Hynes, 1999) have produced the so-called "decoupled approaches". The steps to perform a decoupled analysis are: 1) estimate the average acceleration time response executing the dynamic response of the slope assuming that failure does not occur, and 2) use the equivalent input motion into the classical rigid block method to calculate permanent displacements (Jibson, 2010). This two-stage decoupled approach is not the most realistic representation of the slope behavior to include dynamic response of the slope to compute seismic displacements because, in nature, the slope dynamic motion also evolves with the failure response. Finally, the "fully coupled approaches" accomplish a simultaneous analysis of the deformations caused by the dynamic response (in 1D or 2D directions) and the sliding response (Bray, 2007). They could account for plastic deformations but are computationally more costly than the rigid block and decoupled methodologies (Jibson, 2010).

2.4. Stress Deformation Analysis

Sloped earthworks and most geotechnical problems can be modeled based on theoretical descriptions of the materials mechanics and boundary conditions. They can be represented in terms

of a set of governing equations, which are complex systems of differential equations. The problem then is purely mathematical, which in most cases needs the simplification of the model's boundary conditions and material behavior in order to be solved. Therefore, analytical solutions are very limited, or otherwise misrepresentative, and a numerical approach is required.

Stress-deformation analysis is a relatively new category to assess seismic slope stability, which comprises a number of numerical techniques designed to approximate the solution of boundary value problems. The problem domain is discretized in small pieces, and the governing equations are solved for a finite number of points. Soil behavior can be characterized by complex constitutive models (see Figure 4) and by seismic loads in terms of acceleration or stress time-history. In general, stress-deformation analyses allow realistic representations (properties, geometry, etc.), but they are computationally expensive.

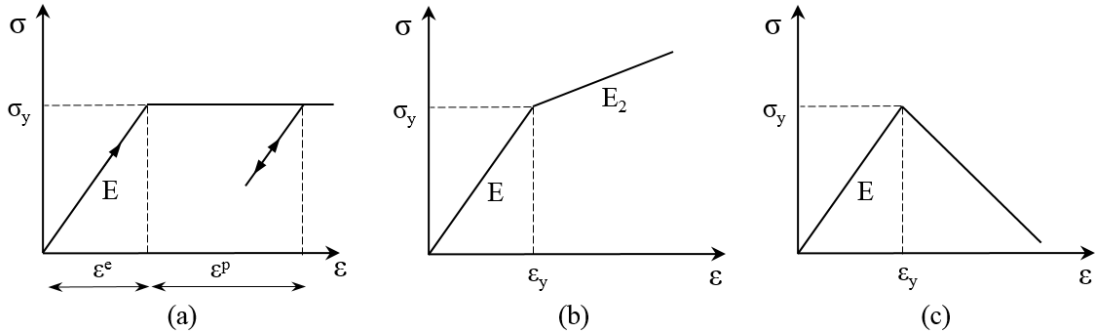

Figure 4. Stress-strain relationships. (a): Elastic perfectly plastic, (b): Elastic-linear hardening, (c): Elastic-linear softening

The stability analysis is based on estimating the strength reduction factor (SRF), which resembles a factor of safety. In this approach, the shear strength parameters are reduced by dividing them by the SRF until failure is reached (the solution does not converge).

One of the earliest investigations that utilized numerical methods in engineering was performed by Clough in 1960 (Jibson, 2010). Duncan (1996) presents a list of pioneer authors that used finite element analyses with different stress-strain relationships on static slope stability. Similarly, Kramer (2007) presents different authors that performed dynamic finite element analyses of slopes (e.g. Seed (1973), Lee (1974), Serff et al. (1976), Finn et al. (1986), etc.) More recently, Khosravi et al. (2013) use finite element models to compare approaches to perform seismically loaded slopes. Fotopoulou and Pitilakis (2015) developed empirical predictive equations using the finite

differences method.

The advent of more advanced computational tools and new numerical techniques signified that two broad stress-strain numerical approaches can be distinguished: mesh-based methods and particle-based methods. Mesh-based methods such as the Finite Element Method (FEM) or the Finite Differences Method (FDM) are the most common techniques, and the main characteristic is that the material properties are referenced to a deformable mesh. One limitation of mesh-based methods is that they suffer from mesh tangling when large deformations are involved. Thus, these approaches are efficiently applied to mesh distortions that do not compromise the convergence condition; therefore, a stress reduction factor (SRF) could be estimated, or a performance evaluation based on allowable deformations could be carried out. Otherwise, it can be assumed that failure has occurred, and the post-failure analysis (run-out processes) requires numerical approaches capable of dealing with large deformations such as the particle-based methods. Examples of these numerical techniques are the Material Point Method (MPM) and the Smoothed Particle Hydrodynamics (SPH) which are Lagrangian descriptions that carry the material properties as a set of material points (Yerro et al., 2016), and they are adequate to simulate large deformations and study the post-failure soil behavior as well as 'flows' or 'lateral spreads' type of landslide movements.

2.5. Conclusion

The most well-known methods to analyze slope stability considering dynamic loads were presented. The first approach was established by Terzaghi and it is called pseudo-static analysis. The basic concept of this method is the introduction of a horizontal load equal to the weight of the block or sliding mass times the seismic coefficient k_s. Then, a conventional static slope stability analysis is performed to find a factor of safety. Another methodology is the sliding-block analysis introduced by Newmark, which is currently one of the most common in engineering practice. This method involves two integrations: a first integration of the acceleration time record that surpasses the yield acceleration (A_y), which is the seismic coefficient that yields a safety factor equal to one, and a second integration to find permanent displacements. The third method is the stress-deformation analysis, which consists of applying numerical techniques with sophisticated

constitutive soil behavior models to solve a set of governing equations. In this method, we can distinguish mesh-based methods (e.g., FEM, FDM) and particle-based methods (e.g., MPM, SPH).

Sliding-block methods can be adequate to estimate deformations resulting from slides type of movements which include rotational and translational landslides. These movements can also be represented using numerical methods; however when large deformations are involved (e.g. lateral spreads and flows) particle-based numerical techniques are required.

Finally, this study has identified: a) how the different methodologies evaluate the onset of failure (stability analysis) and b) the applicability of these methods to predict post-failure deformations and final run-outs (post-failure analysis). Table 1 summarizes the findings.

Table 1. Summary of the applicability of the methods on a) stability and b) post-failure analysis.

	Pseudostatic Analysis	Sliding Block Analysis	Stress Deformation Analysis
Stability Analysis	Factor of Safety FS >1	Allowable permanent displacements	Strength Reduction Factor SRF > 1
Post failure analysis (Risk analysis)	Not applicable	Constrained to small deformations	Applicable (Large run-outs only with particle-based methods)

CHAPTER 3. SEISMIC SLOPE STABILITY: A COMPARISON STUDY OF EMPIRICAL PREDICTIVE METHODS WITH THE FINITE ELEMENT METHOD

3.1. Introduction

In chapter 2, the methods to assess seismic slope stability were presented. These methods can be classified into three groups: the pseudostatic method, the sliding-block methods, and the stress-strain numerical methods. Each one of them presents advantages and disadvantages. The pseudostatic method is simple to apply, but a factor of safety as the sole criteria of stability evaluation is not sufficient for post-failure analysis. On the other hand, the stress-strain methods, also known as stress-deformation or numerical methods, could represent the dynamic soil behavior with high sophistication, but the computation time efficiency is forsaken. The Newmark methods or sliding-block approaches qualify as a link between the other two methods because they are neither too simple nor too complex to compute permanent displacements (Jibson, 2010).

Over the last three decades, some major developments in seismic slope stability are the use of displacements as criteria of performance evaluation, and the acceptance of the numerical platforms, e.g., FLAC (finite difference approach) and Plaxis (finite element approach), for dynamic analysis (Finn, 2013). Recently, numerical frameworks that account for large deformations (e.g., the Material Point Method) are also being incorporated into dynamic analyses (e.g., Bhandari et al., 2016, Zabala et al., 2007). Since the sliding block methods and the stress-strain numerical methods provide seismic displacements, they have extensively been studied, and as a result, empirical predictive equations, also called ground motion prediction equations (GMPE) or attenuation relationships, were formulated for the prediction of seismically induced displacements as functions of ground motion parameters, also referred as intensity measures (IM). Furthermore, as mentioned in Chapter 2, sliding-block methods are adequate to represent displacements from ‘slides’ type of landslides, meanwhile stress-deformation numerical methods can be capable to represent not only ‘slides’ type of movements, but also processes including large deformations such as ‘flows’. In particular, this research is focused on ‘slides’ given the characteristics presented on a previous study on a shaking-table test.

Identifying where earthquakes are going to happen is uncertain, and this restricts engineers from knowing where to invest in field instrumentation to study seismic effects (Kutter, 1995). Therefore,

the use of scale models is important for data collection to apply them in geotechnical modeling. In this investigation, a scale model tested on a shaking table by Hiraoka et al. (2013) and studied numerically by Bhandari et al. (2016) is used for validation and scaled up to prototype proportions to evaluate its response to a dataset of seismic records to find seismic displacements through the application of empirical prediction methods and the finite element method. The empirical methods include the approaches developed by Newmark (1965), Makdisi and Seed (1978), Hynes-Griffin and Franklin (1984), Bray and Travasarou (2007), Jibson (2007), Hsieh and Lee (2011), and Fotopoulou and Pitilakis (2015). The numerical model is implemented in Plaxis2D using a linear elastic perfectly plastic stress-strain constitutive law with the Mohr Coulomb failure model. These results are compared statistically, and new empirical approaches to calculating seismic displacements are proposed.

3.2. Methodology

The study consists of the seismic slope analysis of granular material using twelve empirical prediction equations and the finite element method (FEM). A shaking-table model previously studied is used for numerical validation and scaled up to a prototype model; then, it is subjected to 88 acceleration time records obtained from the Pacific Earthquake Engineering Research (PEER) database with moment magnitudes (M) ranging from 6 to 7.62 and rupture distances (R) from 0.2 to 180.2 km. The permanent seismic displacements obtained using the empirical approaches are compared statistically to FEM results using a rating technique similar to Jafarzadeh et al. (2019). Then, seven ground motion parameters are computed and correlated to the horizontal displacements obtained from the finite element (FE) model to observe the best correlations and propose new empirical correlations to reckon seismic displacements. Figure 5 displays the general methodology adopted for this study.

3.2.1. Prototype and scale model characteristics

A previous study of a small slope on a shaking table experiment from Hiraoka et al. (2013) was considered for reference. The scale model (H=0.5 m and 45° slope inclination) comprised a granular soil with friction angle ϕ=23.5° and cohesion c=0.78 kPa. This experiment was investigated numerically with the 2D smoothed particle hydrodynamics (SPH) model (Hiraoka et al., 2013). Likewise, Bhandari et al. (2016) performed a numerical study of this test using the finite

element method (FEM) and the material point method (MPM). In this research, the same scale model was simulated with Plaxis (FEM software) and the results were compared with the previous publications for validation.

After this validation, the geometry and material properties from the model were scaled up to a prototype slope to apply the empirical equations and to implement a real scale FEM model. A multiplier factor, λ=10, was used for scaling up the dimensions to represent the proportions of typical embankments and minimize the gravity effects of scaling. The soil properties were selected iteratively to be consistent with the inclination of the slope and to ensure static slope stability while maintaining the factor of safety similar to the scale model. Ignoring the adjustment to the scale material properties would result in an unstable structure failing by self-weight. The final shear strength parameters required to ensure the static stability of the prototype slope are c=2.4 kPa and ϕ=46.5°, and they represent typical values of glacial tilts or heavily compacted materials. The prototype dimensions are representative of a typical embankment or a disposal landfill where deep failure planes are not considered for the design.

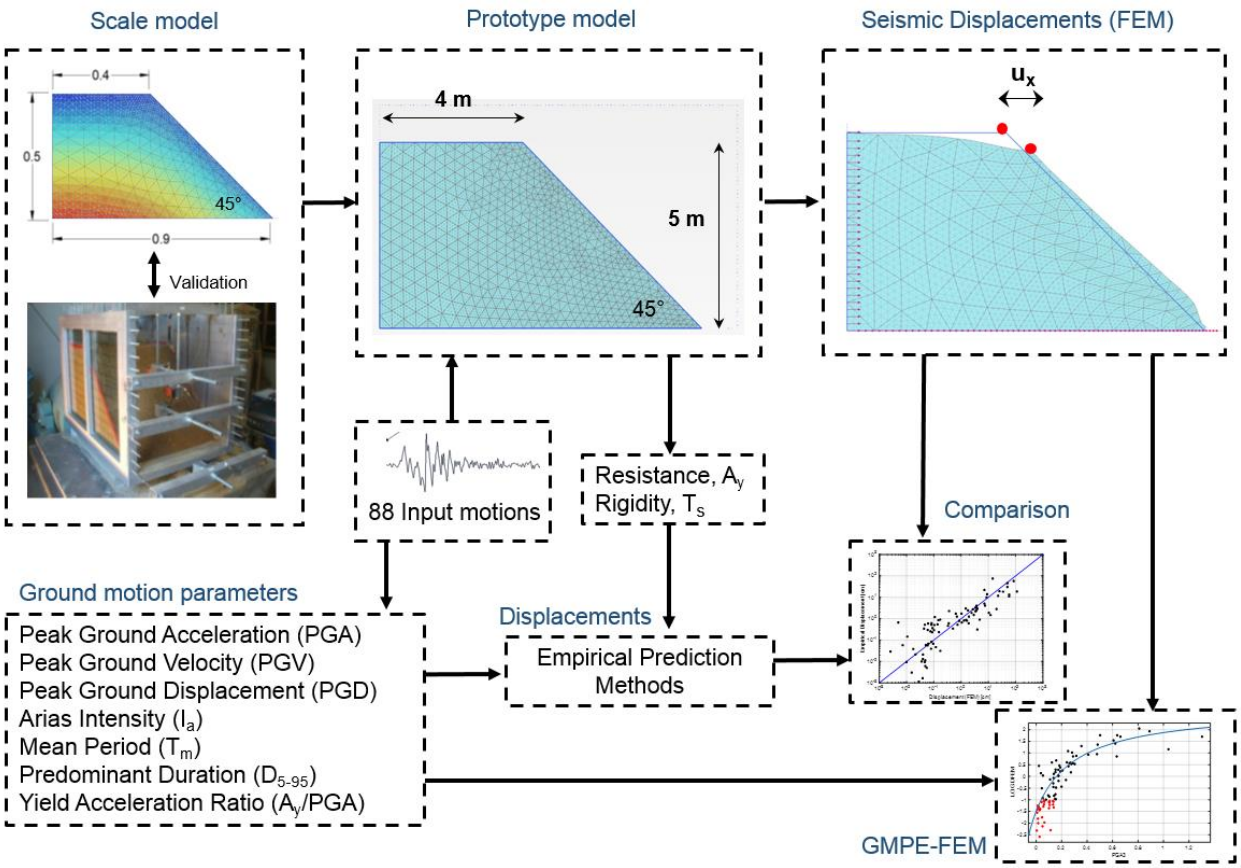

Figure 5. Flowchart of methodology

3.2.2. Dynamic resistance and rigidity of the slope

Pseudostatic analyses were carried out with different seismic coefficients (k) to calculate the yield acceleration (A_y), which represents the dynamic resistance of the slope. The analyses were completed using the ordinary method of slices (OMS) and adopting circular slip surfaces with the Mohr Coulomb failure criterion. Figure 6 displays the reduction of the factor of safety with respect to the seismic coefficient. A higher seismic coefficient corresponds to greater induced stress; thus, the slope tends to be more unstable, and it is reflected on a reduction of the safety factor. The yield coefficient (k_y) of the slope is 0.248; then, the yield acceleration is 0.248g or 2.432 m/s^2.

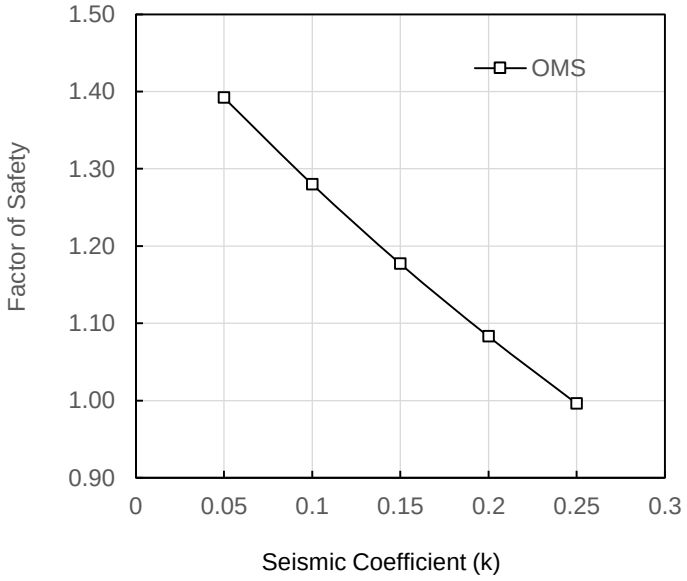

Figure 6. Factor of safety vs. seismic coefficient

Another important parameter used in the empirical methods is the fundamental period of the structure (T_s), which provides an idea of the rigidity of the slope: stiff for T_s<0.2 s, and flexible otherwise (Fotopoulou and Pitilakis, 2015). It can be calculated by $T_s=4H/V_s$, where H is the height equal to 5 m, and V_s is the shear wave velocity equal to 110 m/s. In this case, T_s is found 0.18 s.

3.2.3. Earthquake ground motions

A total of 88 seismic records have been utilized in the analysis (summarized in Appendix A). The input motions correspond to moment magnitudes (M) between 6 to 7.62, rupture distances (R) between 0.21 to 180.24 km, and shear wave velocities in the upper 30 meters (Vs_{30}) ranging from

406.7 to 595.2 m/s. Seven intensity measures (IM) were computed from the acceleration time records: peak ground acceleration (PGA) with values varying from 0.004g to 1.30g, peak ground velocity (PGV) values varying from 0.76 to 106.82 cm/s, peak ground displacement (PGD) varying from 0.17 to 53.76 cm, Arias intensity (I_a) varying from 0.04 to 996.67 cm/s, mean period (T_m) varying from 0.18 to 1.64 seconds, predominant duration ($D_{5\text{-}95}$) varying from 2.55 to 37.58 seconds, and the yield acceleration ratio (A_y/PGA) ranging from 0 to 50.16. Histograms of intensity measures and plots correlating ground motion parameters are presented in Appendix B and C, respectively. Similarly, Figure 7 plots the Fourier amplitude spectra and the response spectral acceleration of the input loads. All these parameters are used in the calculations of the horizontal seismic displacement.

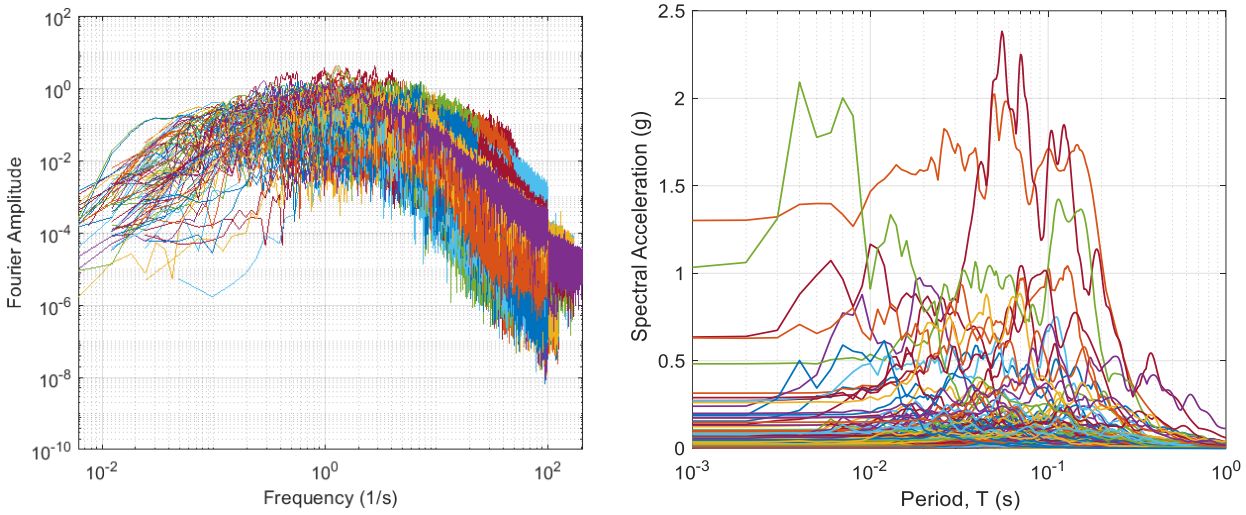

(a) (b)

Figure 7. (a) Fourier Amplitude Spectra, and (b) Response Spectral Acceleration

3.2.4. Empirical Predictive Approaches

Twelve empirical predictive approaches were considered. The study includes the Newmark-type methods (rigid, decoupled, coupled), and numerically developed empirical approaches proposed by different authors. As explained in section 2.3, the complexity of each method varies. Table 2 summarizes the methods used in this study.

Rigid methods

The classical Newmark method or rigid block method (1965) was implemented in this research using a Matlab code that begins integrating the ground acceleration that exceeds the yield acceleration in an acceleration time record and stops when the relative velocity is zero as shown in Figure 2. Only the positive side of the accelerations are considered for the integration, so upslope displacements are neglected (See Figure 8).

Two empirical rigid methods developed by Jibson (2007) are considered in this study and presented in Equations 6 and 7. The horizontal displacement (D) in centimeters is calculated as a function of Arias intensity (I_a) in meters per second, the yield acceleration (A_y) in g, and the yield acceleration ratio (A_y/A_{max}). These relationships are recommended to be applied to slopes (natural or man-made) with shallower landslides in brittle materials and for yield accelerations between 0.2 and 0.8 g.

$$\mathrm{Log(D)} = 2.401\log(\mathrm{I_a}) - 3.481\log(\mathrm{A_y}) - 3.230 \pm 0.656 \qquad (6)$$

$$\mathrm{Log(D)} = 0.561\log(\mathrm{I_a}) - 3.833\log(\mathrm{A_y/A_{max}}) - 1.474 \pm 0.616 \qquad (7)$$

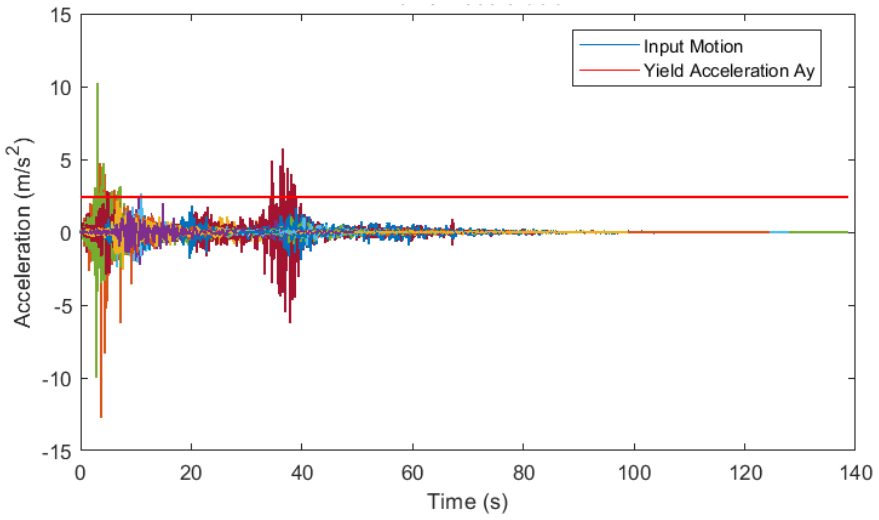

Figure 8. Acceleration time records and yield acceleration used in the study

As it will be seen later in Equation 15, the simplified approach to estimate seismic displacements presented by Bray and Travasarou (2007) is function of the degraded spectral acceleration (S_a) at $1.5T_s$, where T_s is the fundamental period of the slope, the yield coefficient (k_y) in g, and the

moment magnitude (M). This approach can be used as an equivalent rigid approximation (Equation 8) by estimating the spectral accelerations (S_a) corresponding to slope structures that have fundamental periods (T_s) equal to zero, namely estimating the displacement as a function of the PGA. The non-zero displacements D are in cm and PGA in g.

$$\mathrm{Log(D)} = -0.22 - 2.83\ln(k_y) - 0.333[\ln(k_y)]^2 + 0.566\ln(k_y)\ln(\mathrm{PGA}) + 3.04\ln(\mathrm{PGA}) - 0.244[\ln(\mathrm{PGA})]^2 + 0.278(\mathrm{M}-7) \pm \varepsilon \quad (8)$$

The final rigid approach included is from Hsieh and Lee (2010), which incorporates corrections to linearity correlations among the yield acceleration, Arias intensity, and displacements previously studied by Jibson (2007). In this study, the form II (Equation 9) of their empirical method is used, which corresponds to a global data set correlation where D is in cm, I_a m/s, and A_y in g.

$$\mathrm{Log(D)} = 0.847\log(I_a) - 10.62A_y + 6.587A_y\log(I_a) + 1.84 \pm 0.295 \quad (9)$$

Decoupled methods

Two decoupled procedures were considered. The Makdisi and Seed (1978) approach and the Hynes-Griffin and Franklin (1984). The decoupled Newmark method was explained in section 2.3 The Makdisi and Seed (1978) was formulated using a dynamic finite element method to account for the dynamic displacements (Seed 1979, Jibson 2010). The dynamic response analysis consisted of embankments and dams with heights between 30 and 180 m and with shear wave velocities between 92 and 300 m/s. The following charts (Figure 9) were developed to estimate the permanent displacements as a function of the yield acceleration A_y, the maximum horizontal equivalent acceleration (MHEA), magnitude, and the depth of potential failure.

For this approach, it was necessary to calculate the maximum crest acceleration. There is uncertainty in estimating this value (Jibson 2010), and in this study, the shear beam approach described in Kramer (2017) and lecture notes of Bartlett (2011) were applied.

$$\ddot{u}_{max} = \sqrt{\sum_{n=1}^{3}(\phi_n(y)\cdot Sa_n)^2} \quad (10)$$

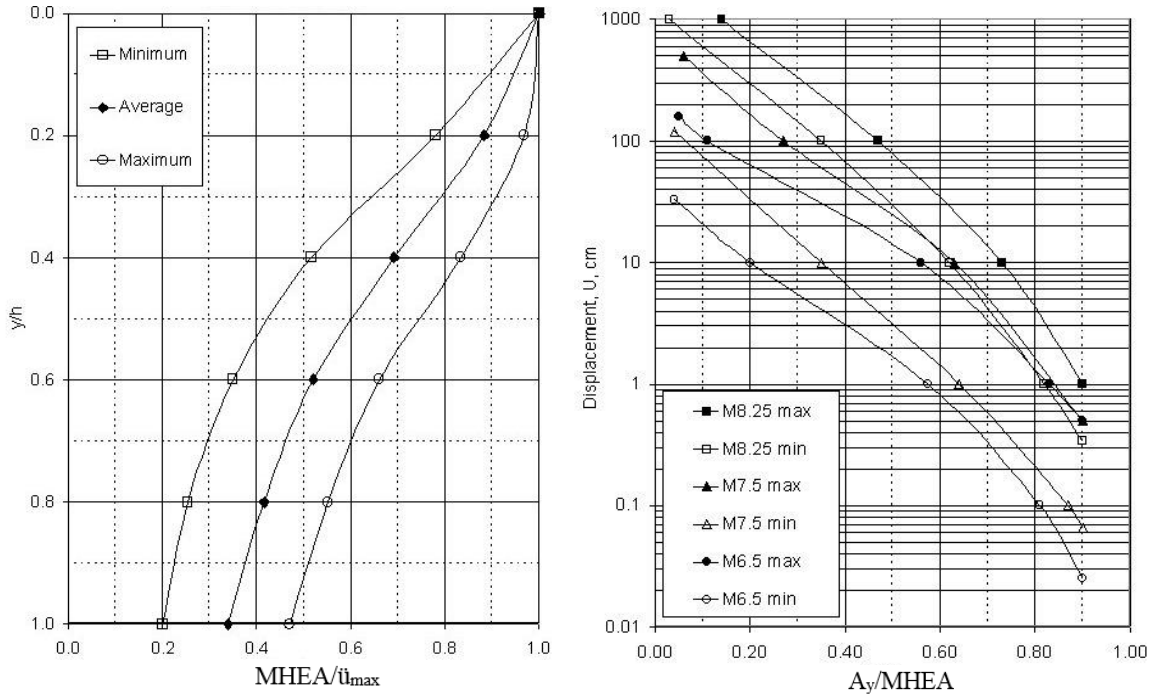

(a) (b)

Figure 9. (a): Variation of maximum acceleration ratio with depth of sliding mass. (b): Variation of permanent displacement with respect to yield acceleration/MHEA. (Makdisi and Seed, 1978)

The max crest acceleration was estimated using Equation 10. Where $\phi_n(y)$ values are the mode participation factors for the first three modes at the crest of the slope (y=0), and they are $\phi_1(0)=1.60$, $\phi_2(0)=1.06$, and $\phi_3(0)=0.86$ (Bartlett, 2011). Similarly, Sa_n are the spectral accelerations for the fundamental periods corresponding to the first three modes of vibration. These periods were computed using Equation 11, the β-values are $\beta_1 = 2.40$, $\beta_2 = 5.52$, and $\beta_3 = 8.65$, H is the height of the slope, and V_s is the shear wave velocity.

$$T_n = \frac{2\pi}{\beta_n}\frac{H}{V_s} \qquad (11)$$

Calculating the periods with the β-values and replacing it in Equation 10, the max crest acceleration was approximated using the following Equation 12:

$$\ddot{u}_{max} = \sqrt{\left[1.60 \cdot S_{a1\,(T_s=0.1188\ s)}\right]^2 + \left[1.06 \cdot S_{a2\,(T_s=0.0517\ s)}\right]^2 + \left[0.86 \cdot S_{a3\,(T_s=0.0322\ s)}\right]^2} \qquad (12)$$

Then, the maximum horizontal equivalent acceleration (MHEA) was calculated applying Figure 9a and adopting failure surfaces at the base of the slope; therefore, the ratio y/H equals one and the MHEA is 0.35 of the max crest acceleration ($\ddot{u}_{max}$). Afterwards, Figure 9b was used to calculate the horizontal permanent displacement. This process was implemented in Matlab.

In addition, the Hynes-Griffin and Franklin (1984) decoupled approach was applied. This model considers the amplification of a triangular wedge with an underlain foundation settled on a bedrock layer. The functional form of this approach is dependent on the yield acceleration ratio (A_y/A_{max}), which is calculated based on Equation 13 (Meehan and Vahedifard, 2013) where D is in cm. This approach incorporates the amplification response of bedrock ground motions through the slope.

$$\log(D) = -0.116\cdot\left(\frac{A_y}{A_{max}}\right)^4 - 0.702\cdot\left(\frac{A_y}{A_{max}}\right)^3 - 1.733\cdot\left(\frac{A_y}{A_{max}}\right)^2 - 2.854\cdot\left(\frac{A_y}{A_{max}}\right) - 0.287 \qquad (13)$$

Coupled method

The fully coupled model from Bray and Travasarou (2007) was considered in this analysis. This procedure uses a nonlinear fully coupled stick-slip deformable slope model that incorporates a more accurate dynamic response of the slope and the sliding mass deformation caused by the seismically induced deviatoric shearing. The model characterizes the slope displacements as a function of its dynamic strength and stiffness, which are represented respectively by the slope's yield coefficient (k_y), and its initial fundamental period (T_s). This methodology consists of two stages: 1) calculating the probability of negligible zero-displacement (Equation 14) and 2) calculating the amount of non-zero displacement (Equation 15). This formulation has been idealized for k_y values ranging from 0.02 to 0.4, and T_s values from 0 to 2 s (obtained by varying the height of a sliding block between 12 and 100 m and shear velocity, V_s, between 200 and 425 m/s), and it has proven to provide consistent results for earth dams and solid-waste landfills. For this study, the predictive equation which is not biased by magnitude is employed to estimate the displacements.

$$P(D=0)=1-\phi\left[-1.76-3.22\ln(k_y)-0.484T_s\ln(k_y)+3.52\ln(S_a(1.5T_s))\right] \qquad (14)$$

$$\ln(D) = -1.10 - 2.83\ln(k_y) - 0.333[\ln(k_y)]^2 + 0.566\ln(k_y)\ln(S_a(1.5T_s)) + 3.04\ln(S_a(1.5T_s)) - 0.244[\ln(S_a(1.5T_s))]^2 + 1.50T_s + 0.278(M-7) \pm \varepsilon \quad (15)$$

The first term of Equation 15 must be replaced with -0.22 when T_s<0.05 s. ε=normally distributed random variable with zero mean and standard deviation σ=0.67.

Numerically developed empirical method

Finally, empirical stress deformation predictive equations developed by Fotopoulou and Pitilakis (2015) using non-linear numerical analyses and the finite difference method (FDM) in the FLAC2D interface were employed. The predictive equations are presented as functions of different intensity measures and resulted from a parametric study of slopes with heights from 20 to 40 m, shear velocities from 150 to 400 m/s, and underlying stiff clayey soil and another elastic bedrock. The k_y values are between 0.05 and 0.30, and T_s values between 0.032 and 0.69 s.

$$\ln(D) = -9.891 + 1.873\ln(PGV) - 5.964k_y + 0.285M \pm 0.65\varepsilon \quad (16)$$

$$\ln(D) = -2.965 + 2.127\ln(PGA) - 6.583k_y + 0.535M \pm 0.72\varepsilon \quad (17)$$

$$\ln(D) = -10.246 - 2.165\ln(A_y/PGA) + 7.844k_y + 0.654M \pm 0.75\varepsilon \quad (18)$$

$$\ln(D) = -8.076 + 1.873\ln(PGV) + 0.200\ln(I_a) - 5.964k_y \pm 0.61\varepsilon \quad (19)$$

Where the displacements D are in m, PGA in g, PGV in cm/s, and I_a in m/s

Table 2. Empirical Predictive Equations for Seismic Slope Stability

N°	Model	Type	Functional Form
1	Newmark (1965)	Rigid	Original method
2	Makdisi and Seed (1978)	Decoupled	Charts
3	Hynes-Griffin and Franklin (1984)	Decoupled	$\log(D) = -0.116\cdot\left(\frac{A_y}{A_{max}}\right)^4 - 0.702\cdot\left(\frac{A_y}{A_{max}}\right)^3 - 1.733\cdot\left(\frac{A_y}{A_{max}}\right)^2 - 2.854\cdot\left(\frac{A_y}{A_{max}}\right) - 0.287$
4	Bray and Travasarou – 1 (2007)	Coupled	$\ln(D) = -1.10 - 2.83\ln(k_y) - 0.333[\ln(k_y)]^2 + 0.566\ln(k_y)\ln(S_a(1.5T_s)) + 3.04\ln(S_a(1.5T_s)) - 0.244[\ln(S_a(1.5T_s))]^2 + 1.50T_s + 0.278(M-7) \pm \varepsilon$
5	Bray and Travasarou – 2 (2007)	Rigid	$\mathrm{Log}(D) = -0.22 - 2.83\ln(k_y) - 0.333[\ln(k_y)]^2 + 0.566\ln(k_y)\ln(PGA) + 3.04\ln(PGA) - 0.244[\ln(PGA)]^2 + 0.278(M-7) \pm \varepsilon$
6	Jibson 2 (2007)	Rigid	$\mathrm{Log}(D) = 2.401\log(I_a) - 3.481\log(A_y) - 3.230 \pm 0.656$
7	Jibson 3 (2007)	Rigid	$\mathrm{Log}(D) = 0.561\log(I_a) - 3.833\log(A_y/A_{max}) - 1.474 \pm 0.616$
8	Hsieh and Lee (2011)	Rigid	$\mathrm{Log}(D) = 0.847\log(I_a) - 10.62A_y + 6.587A_y\log(I_a) + 1.84 \pm 0.295$
9	Fotopoulou and Pitilakis – 1 (2015), Method 1	Numerical	$\log(D) = -9.891 + 1.873\ln(PGV) - 5.964k_y + 0.285M \pm 0.65\varepsilon$
10	Fotopoulou and Pitilakis – 2 (2015) , Method 2	Numerical	$\log(D) = -2.965 + 2.127\ln(PGA) - 6.583k_y + 0.535M \pm 0.72\varepsilon$
11	Fotopoulou and Pitilakis – 3 (2015), Method 3	Numerical	$\log(D) = -10.246 - 2.165\ln(A_y/PGA) + 7.844k_y + 0.654M \pm 0.75\varepsilon$
12	Fotopoulou and Pitilakis – 4 (2015), Method 4	Numerical	$\log(D) = -8.076 + 1.873\ln(PGV) + 0.200\ln(I_a) - 5.964k_y \pm 0.61\varepsilon$

3.2.5. Finite Element Model

The stress-strain numerical analysis was performed using the finite element method (FEM) with the Plaxis software. The contour area extends from 0 to 10 meters in the x-direction and 0 to 6 meters in the y-direction. The slope is 5 m high and inclined 45° with respect to the horizontal. Plane strain conditions are imposed with 15-noded elements and mesh sizes ranging from 0.20 m in zones closer to the slope, 1.20 m in the boundaries, and an average of 0.546 m. The total number of elements and number of nodes are respectively 445 and 3663. The average mesh size was selected under two criteria: the computation time's optimization and the suggestion of the Plaxis manual from Kuhlmeyer and Lysmer (1973) to assume one-eight of the wavelength related to the maximum frequency content (f_{max}) as shown in Equation 20. The maximum frequency (Nyquist frequency) varies for each input motion, and for this study an f_{max} = 25 Hz is adopted and selected based upon the Fourier amplitude spectra corresponding to a value close to zero (Figure 7a). This yields an average length of 0.55 m.

$$\text{Average Element Size} \leq \frac{\lambda}{8} = \frac{V_s}{8f_{max}} \qquad (20)$$

Two construction phases have been used in the analysis. The initial phase consisted of initializing the stresses due to gravity loading (see Figure 10). In this stage, the left side is free in the y-direction and fixed in the x-direction; the rigid base of the slope is free in x-direction and fixed in y-direction. The second stage is the dynamic phase where the seismic load is prescribed at the base and the left side of the model. Dynamic multipliers and the prescribed line displacement options are applied in the x-direction at the base and left side boundaries of the slope. This implies that the slope lays on a rigid base (e.g. bedrock). Considering a rigid boundary at the base means that elastic waves are trapped in the embedded material because they reflect at the boundary. In addition, the assumption that the lateral boundary moves with the same input acceleration time history is realistic for the shaking table analysis, but is less representative of flexible slopes. The dynamic time interval is set equal to the duration of the recorded input motion. Finally, it is important to note that for all cases, the slope becomes stable meaning that the recorded displacement stabilizes during the dynamic loading stage. The horizontal movement at the crest of the slope is considered for reference (see some examples of displacement vs time plots in Figure 12).

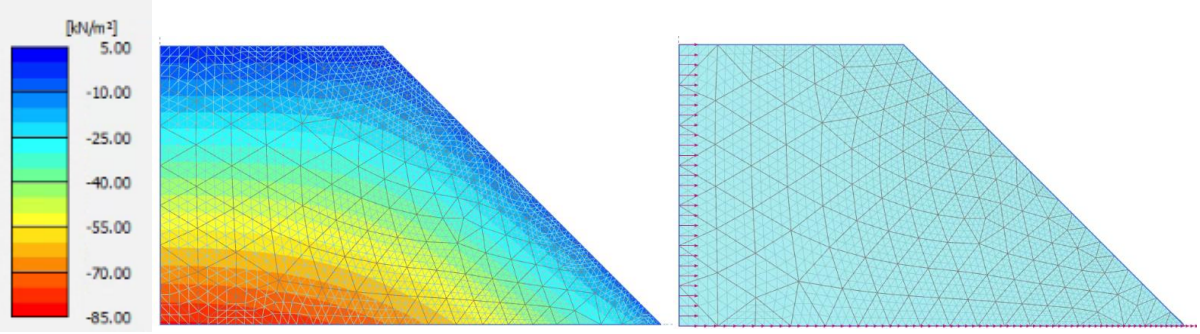

(a) (b)

Figure 10. (a) Initial effective vertical stresses, and (b) prescribed line displacement on mesh

The Mohr Coulomb failure mode for drained conditions with zero tension cut-off, friction angle 46.5°, cohesion 2.40 kPa, and linear elastoplastic stress-strain soil behavior has been adopted with a non-associated flow rule with the angle of dilation $\psi = 0$. Based on the shear wave velocity V_s=110 m/s, the shear modulus (G) and the Young modulus (E) were back-calculated using Equations 21 and 22. Table 3 summarizes the material properties.

$$V_s = \sqrt{\frac{G}{\rho}} \qquad (21) \qquad\qquad G = \frac{E}{2(1+\nu)} \qquad (22)$$

Table 3. Material properties

Parameter	**Symbol**	**Unit**	**Value**
Friction angle	ϕ	°	46.5
Cohesion	c	kPa	2.40
Poisson ratio	ν	-	0.33
Young modulus	E	MPa	54.14
Dilatancy	ψ	°	0
Tension cutoff		kPa	0
Shear modulus	G	MPa	20.35
Unit weight	γ	kN/m^3	16.5
Initial porosity	n	-	0.33

3.3. Results

The estimated maximum displacements obtained from the empirical methods and the finite element model are summarized in Appendix D. Table 4 presents the maximum permanent displacement of all the input motions for each of the empirical approaches along with their FEM horizontal displacements and record number. All the models converged until the last dynamic step and the final mesh configurations were not tangled. The maximum permanent displacements calculated from the empirical approaches varies from 0.13 cm to 286.53 cm corresponding to the Hynes-Griffin and Franklin (1984) and the Fotopoulou and Pitilakis – 4 (2015), respectively.

Table 4. Maximum permanent displacements calculated from empirical approaches along with the corresponding displacement obtained with FEM for the same ground motion record.

Approach	Displacement (cm)		Record
	Maximum	FEM	
Newmark (1965)	50.16	112.20	28
Makdisi and Seed (1978)	36.21	58.00	53
Hynes-Griffin and Franklin (1984)	0.13	50.01	2
Bray and Travasarou – 1 (2007)	15.44	112.20	28
Bray and Travasarou – 2 (2007)	29.36	50.01	2
Jibson 2 (2007)	18.88	85.10	79
Jibson 3 (2007)	41.40	50.01	2
Hsieh and Lee (2011)	48.26	85.10	79
Fotopoulou and Pitilakis – 1 (2015)	48.45	49.80	75
Fotopoulou and Pitilakis – 2 (2015)	60.75	14.50	73
Fotopoulou and Pitilakis – 3 (2015)	74.97	14.50	73
Fotopoulou and Pitilakis – 4 (2015)	286.53	112.20	28

The maximum horizontal displacement obtained from the finite element model is 112.20 cm. The results correspond to the input record N° 28 with PGA = 0.809 g, PGV = 1.068 m/s, PGD = 0.159 m, Arias intensity, I_a = 9.291 m/s, mean period, T_m = 0.836 s, predominant duration, $D_{5\text{-}95}$ = 21.76 s, and yield acceleration ratio, A_y/PGA = 0.306. This record also produces the maximum horizontal displacements by means of the Newmark (1965), Bray and Travasarou – 1 (2007), and Fotopoulou and Pitilakis – 4 (2015) empirical approaches. The maximum PGA equals 1.303g and corresponds

to the Record N° 2. Similarly, this record yields the maximum horizontal displacements through the Hynes-Griffin and Franklin (1984), Bray and Travasarou – 2 (2007), and Jibson – 3 (2007) empirical procedures.

Figure 11 presents the final deformed mesh for the record N° 28, which gives the maximum FEM displacement. Figure 12 illustrates the different magnitudes of horizontal displacement at the slope crest for the time records N° 28, 55, and 4.

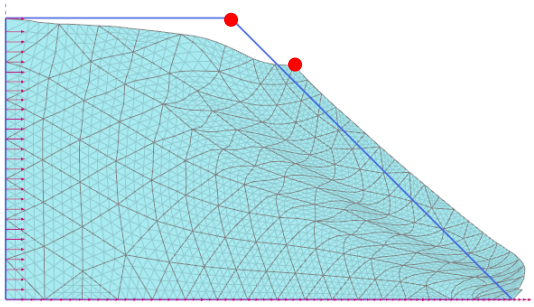

Figure 11. Deformed mesh after FEM dynamic phase subjected to input record N° 28.

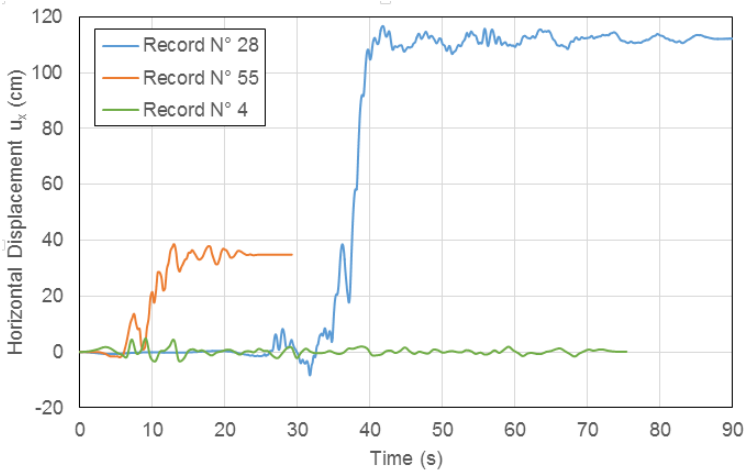

Figure 12. Numerical horizontal displacement versus time for different records.

In Figure 13, it can be seen that the percentage of the computed permanent displacements (D; where the percentage is with respect to the total number of records analyzed) with D>0.1 cm, which for this study are considered to be of engineering significance, ranges from 97.5% for the Fotopoulou and Pitilakis – 4 (2015) to 1.14% for the Hynes-Griffin and Franklin (1984) approach. Similarly, only between 15% and 27.5% of the displacements found using the Newmark (1965), Bray and Travasarou – 1 (2007), Jibson 2 and 3 (2007), and Hsieh and Lee (2011) are bigger than

0.1 cm. For the numerical model, the percentage of the results corresponding to D>0.1 cm is 62.5%. Besides, the cumulative distributions of the FEM results follow a similar trend to all the Fotopoulou and Pitilakis (2015) methods for displacements D>1 cm and to the Makdisi and Seed (1978) for approximately D>5 cm. Thus, Figure 13 lays out a simple way to determine which empirical approach has a better fit with the FEM numerical results. Finally, it can be distinguished that overall permanent displacements obtained from the Bray and Travasarou – 2 (2007), the four Fotopoulou and Pitilakis (2015), and the FEM results are larger than the Newmark (1965), Bray and Travasarou – 1 (2007), Jibson 2 and 3 (2007), and Hsieh and Lee (2011) methods. Histograms of the displacements are presented in Appendix E.

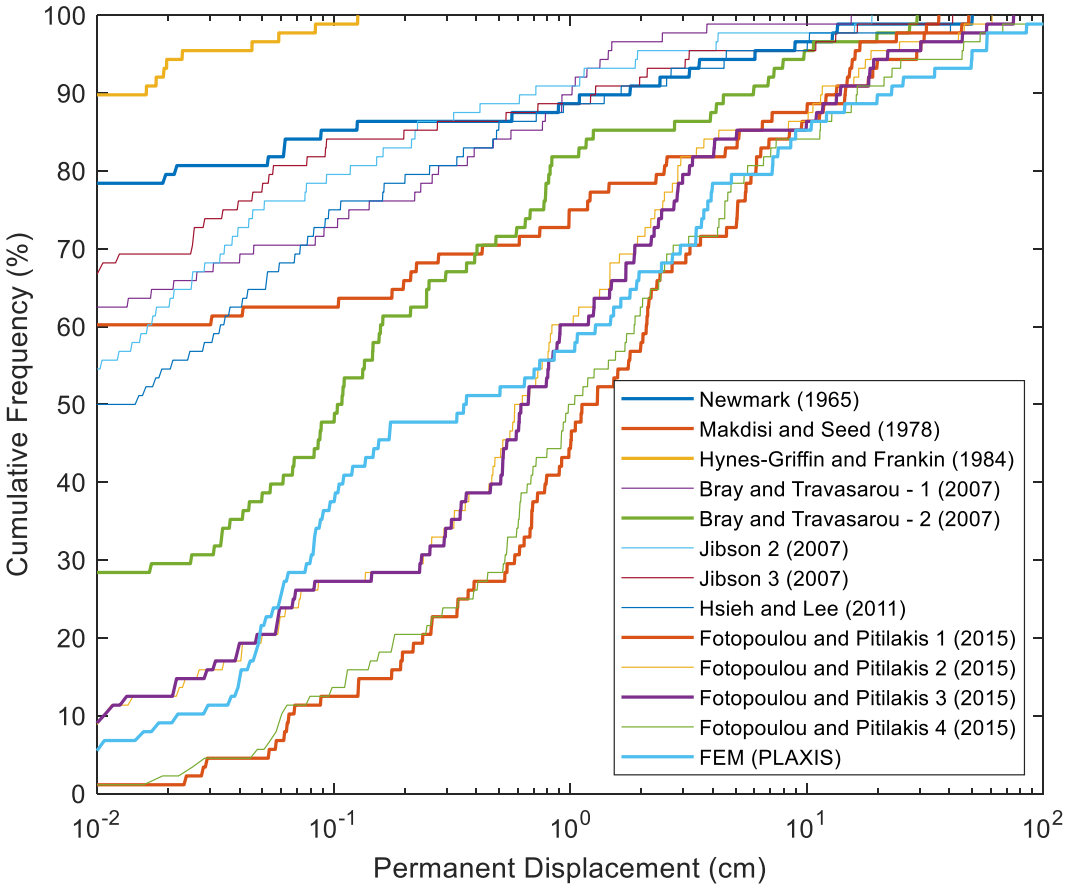

Figure 13. Cumulative frequency versus permanent displacement

CHAPTER 4. DISCUSSION

4.1. Direct Comparison

A direct comparison between the twelve permanent displacements predicted by empirical methods and the FEM horizontal displacements is shown in Figure 14. It can be observed that the numerical results are in good agreement with the Makdisi and Seed (1978), the Bray and Travasarou – 2 (2007), and the Fotopoulou and Pitilakis 2 and 3 (2015) empirical approaches. The Makdisi and Seed approach slightly underpredicts numerical displacements greater than 1 cm. The Bray and Travasarou – 2 (2007) in general underpredicts the FEM results by a factor of one logarithmic scale. The Fotopoulou and Pitilakis (2015) approaches overpredict very small numerical displacements (<1 cm) and underpredict for larger displacements.

The Newmark (1965), Jibson 2 and 3 (2007), and Hsieh and Lee (2011) predict smaller displacements in comparison to the FEM results by approximately the same order of magnitude. This is consistent because the Jibson (2007) and Hsieh and Lee (2011) approaches were developed by applying the classical rigid block method. Finally, the Bray and Travasarou – 1 (2015) or fully coupled method underpredicts permanent displacements compared to the numerical results with high dispersion. This could be because the non-rigid coupled model was developed for earth dams with heights greater than 12 m and for slopes characterized as flexible (higher fundamental periods). The fundamental period of the slope is T_s=0.18 s which classifies it in the range of rigid slope behavior. This is corroborated by a more uniform correlation of permanent displacements for the Bray and Travasarou – 2 (2015) for rigid slopes.

Also, the Hynes-Griffin and Franklin underpredicts considerably the numerical results at least by a factor of one logarithmic scale. It is important to mention that the functional form of this method was presented by Meehan and Vahedifard (2013).

The Newmark (1965), Makdisi and Seed (1978), and Hynes-Griffin and Franklin (1984) present fewer data points because they are dependent of the yield acceleration ratio (A_y/A_{max}), and when this value is greater than the unity, (A_y/A_{max}) > 1, the soil strength is assumed not to be exceeded; therefore, the empirical permanent displacements equal to zero. These data points are not plotted on the graphs.

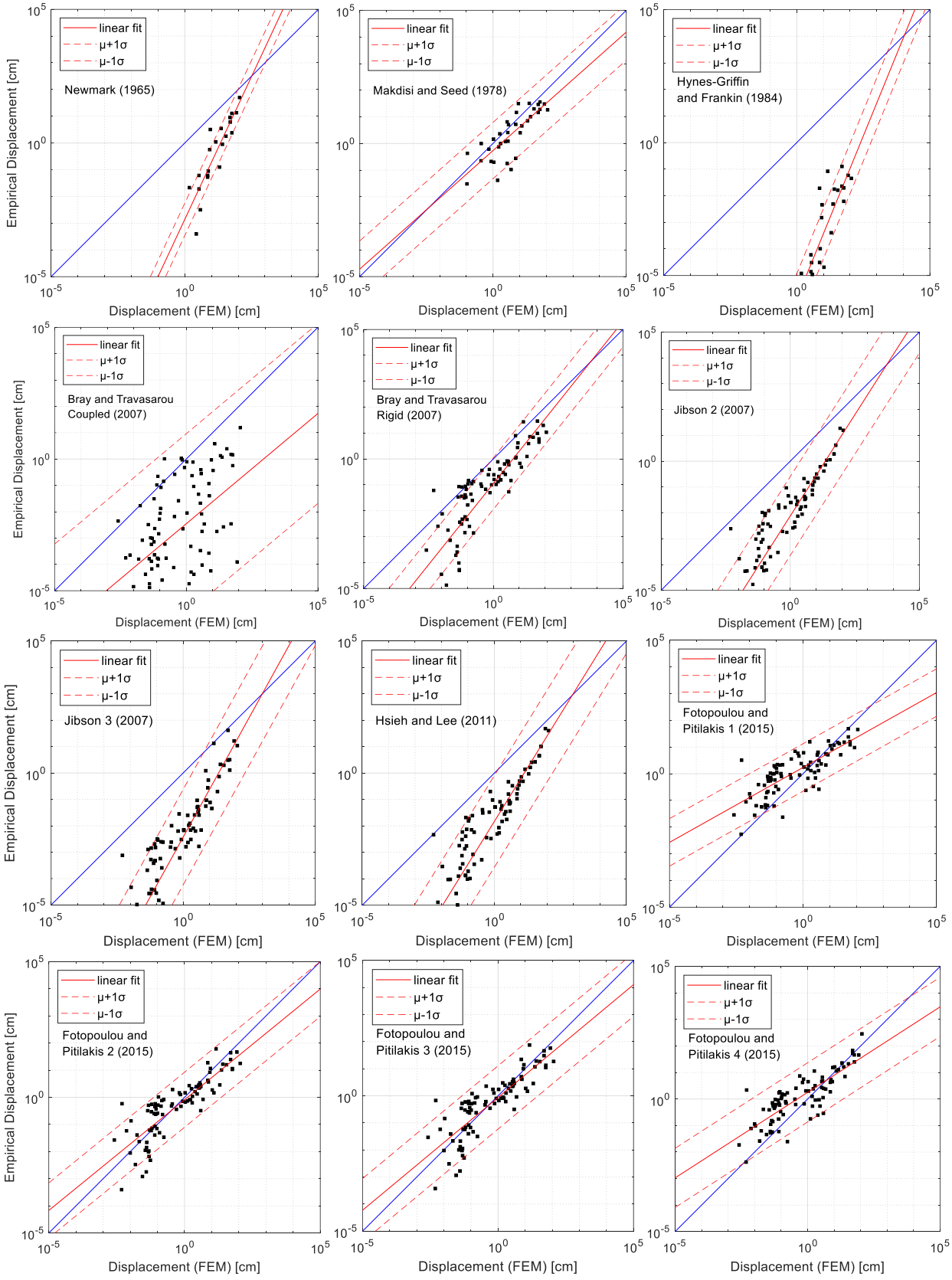

Figure 14. Empirical versus numerical seismic displacements

The overpredictive or underpredictive trend can also be observed in Figure 15, where the cumulative distribution versus the relative difference between FEM and empirical approaches is presented (%Relative Difference= $\frac{D_{numerical}-D_{empirical}}{D_{numerical}} \times 100\%$) . These cumulative distributions were similarly considered to compare different methodologies by Meehan and Vahedifard (2013), and Fotopoulou and Pitilakis (2015). When the relative difference is on the positive side, the empirical method underpredicts the numerical displacements. It can be seen that around 30% or more of results felt on the positive side. About 10% of the Bray and Travasarou – 2 (2007) overpredicts the numerical results, while all data points for the Newmark (1965), Hsieh and Lee (2011), and Jibson 2 and 3 (2007) approaches underpredict the FEM results. These results confirm that rigid approaches do not represent the deformability of the slope resulting in smaller displacements than the values of decoupled or coupled methods. In this regard, it can also be concluded that the rigid methods are nonconservative when they are applied to calculate seismic slope displacements. Also, FEM is generally conservative compared to the empirical approaches since it yields greater displacements, and it is not conservative for small displacements (< 1 cm) when it is contrasted to the Fotopoulou and Pitilakis 1, 2, 3, and 4 (2015) predictive equations.

4.2. Statistical Measures

Four statistical measures were used to assess the fit of the empirical approaches in comparison to the FEM model. These statistical methods employed here were also utilized in the study of Jafarzadeh et al. (2019). They are the Root-Mean-Square Error (RMSE) (Equation 23), the Symmetric Mean Absolute Percentage Error (sMAPE) (Equation 24), the Mean Relative Absolute Error (MRAE) (Equation 25), and the Mean Absolute Scaled Error (MASE) (Equation 26).

$$\mathrm{RMSE} = \sqrt{\frac{\sum(Y_i - F_i)^2}{n}} \qquad (23)$$

$$\mathrm{sMAPE} = \mathrm{mean}\left(200\frac{|Y_i - F_i|}{Y_i + F_i}\right) \qquad (24)$$

$$\mathrm{MRAE} = \mathrm{mean}(|r_i|) = \mathrm{mean}\left(\left|\frac{e_i}{e_i^*}\right|\right) \qquad (25)$$

$$\mathrm{MASE} = \mathrm{mean}(|q_i|) \quad ; \quad q_i = \frac{e_i}{\left(\frac{1}{n-1}\right)\sum_{i=2}^{n}|Y_i - Y_{i-1}|} \qquad (26$$

Where: Y_i is the observed horizontal displacement from the FEM numerical method, F_i is the value from the empirical method, n is the number of elements, e_i is the absolute error, $|Y_i - F_i|$, and e_i^* is the last observation (benchmark method). The results of these statistical methods are summarized in Table 5 and depicted in Figure 16.

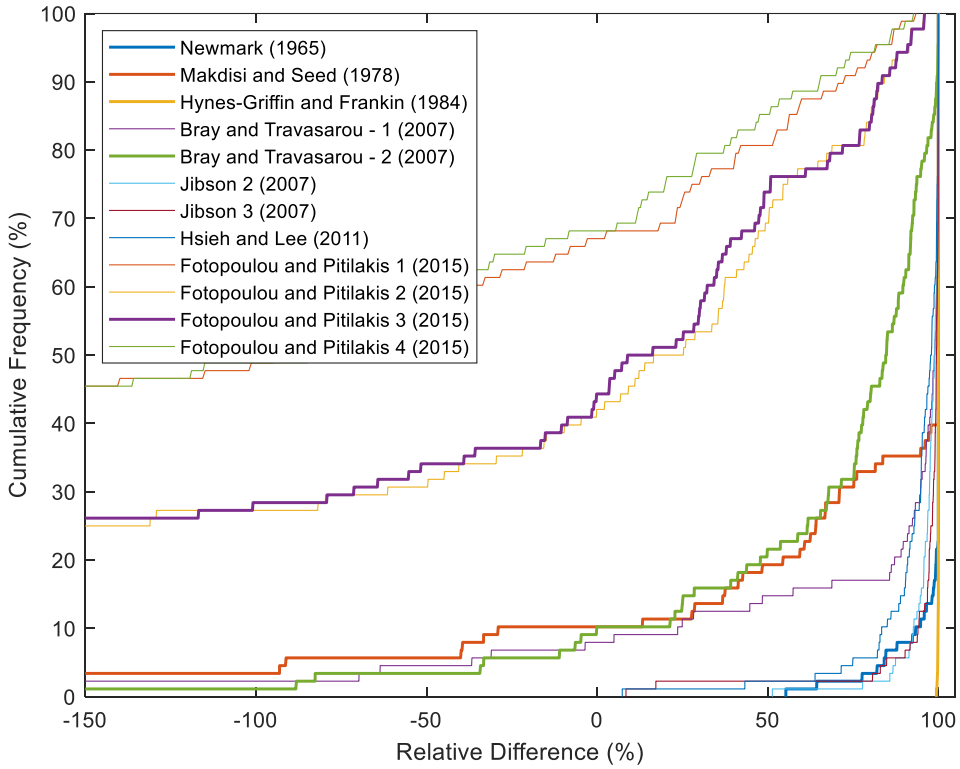

Figure 15. Cumulative distribution of the relative difference between empirically and numerically calculated seismic displacements

Table 5. Summary of statistical errors between numerical and empirical methods

Approach	**Statistical Measure**			
	RMSE cm	**sMAPE %**	**MRAE**	**MASE**
Newmark (1965)	15.447	192.68	17.075	0.76019
Makdisi and Seed (1978)	14.017	156.02	13.786	0.61794
Hynes-Griffin and Franklin (1984)	19.997	199.93	20.353	0.98885
Bray and Travasarou – 1 (2007)	18.844	168.04	19.34	0.9466
Bray and Travasarou – 2 (2007)	16.72	131.83	16.351	0.72803
Jibson 2 (2007)	17.684	189.51	18.704	0.88678

Jibson 3 (2007)	17.396	189.36	17.328	0.77035
Hsieh and Lee (2011)	14.45	179.79	16.238	0.71677
Fotopoulou and Pitilakis – 1 (2015)	13.55	107.42	13.561	0.58438
Fotopoulou and Pitilakis – 2 (2015)	14.656	88.505	13.629	0.54087
Fotopoulou and Pitilakis – 3 (2015)	14.684	87.831	13.363	0.50903
Fotopoulou and Pitilakis – 4 (2015)	19.804	101.64	13.568	0.39854

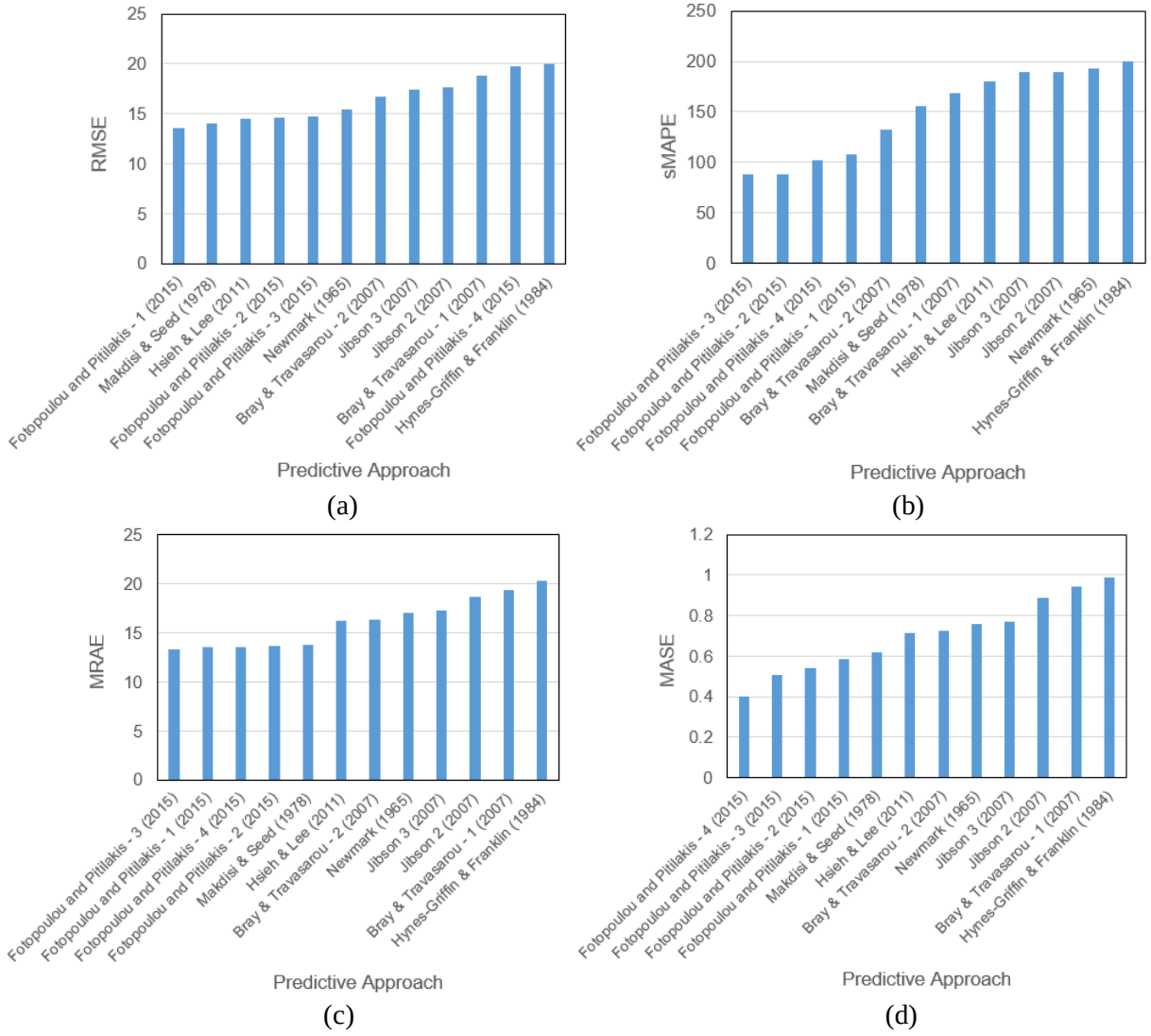

Figure 16. Statistical measures for the empirical predictive approaches.

(a) RMSE, (b) sMAPE, (c) MRAE, and (d) MASE

The RMSE is the standard deviation of the residuals between the numerical and empirical results, and it is a scale-dependent measure that is useful when comparing outputs of different approaches which have the same input dataset (Hyndman and Koehler, 2006). The RMSE values range from 13.55 cm to 19.997 cm corresponding to the Fotopoulou and Pitilakis – 1 (2015) and the Hynes-Griffin and Franklin (1984), respectively. Therefore, considering this measure, the most consistent empirical method with the numerical method is the Fotopoulou and Pitilakis – 1 (2015). Narrowly, the second-best empirical approach is the Makdisi and Seed (1978) with RMSE = 14.017 cm.

The sMAPE is a measure based on percentage errors and it has the advantage of performing better when the observed values Y_i are small or tends to zero (Hyndman and Koehler, 2006), and this statistical measure is more stable when the results have a logarithmic trend (Swanson, Tayman and Barr, 2000; Hyndman and Koehler, 2006) such as the current correlations. Again, it is seen that the Hynes – Griffin and Franklin (1984) predictive approach performs unsatisfactorily in comparison to the other empirical approaches with a sMAPE = 199.93%; conversely, the four finite differences Fotopoulou and Pitilakis (2015) methods yielded the best and lowest sMAPE values followed by the Newmark-type Bray and Travasarou – 2 (2007) approach with 131.83%.

The MRAE is another statistical measure based on relative errors in which the relative errors are divided by the forecast error e_i^* obtained from the benchmark method wherein F_i is the last observation (Jafarzadeh et al., 2019). According to Figure 16, the lowest MRAE error corresponds to the four Fotopoulou and Pitilakis (2015) approaches with values around 13.5, and followed by the Makdisi and Seed (1978) procedure with 13.786. The highest MRAE is calculated for the Hynes – Griffin and Franklin (1984) approach with 20.353.

The last statistical measure reckoned is the MASE where errors related to scale are removed. This method is less sensitive to outliers and less variable on small samples (Hyndman and Koehler, 2006). Identical to the previous statistical techniques, the highest MASE value pertains to the Hynes – Griffin and Franklin (1984) method with a value of 0.9888, and the lowest error is calculated for the Fotopoulou and Pitilakis – 4 (2015) with a value of 0.3985.

4.3. Scoring procedure

A procedure to score the methods has been carried out. The methods with the best statistical fitting number are assigned a value of one, and the methods with the lowest statistical accuracy are assigned a zero value. The intermediate values receive a rating based on interpolation. Finally, the average of these results is calculated. The higher the average score an empirical method yields, the more consistent it is with the FEM numerical results. This methodology is presented in the study of Jafarzadeh et al. (2019). According to this approach, the empirical predictive method with the highest average rating is from Fotopoulou and Pitilakis – 3 (2015) with an average of 0.909, and the lowest average rating corresponds to the Hynes – Griffin and Franklin (1984) with an average equal to zero. The best non-numerically developed empirical approach that more accurately predicts the FEM displacements are the Makdisi and Seed (1978) with 0.722, and the Bray and Travasarou – 2 (2007) for rigid soils with 0.533. Table 6 and Figure 17 exhibit the arithmetically averaged scores for each empirical approach.

Table 6. Summary of scored statistical measures

Approach	Rating Process				
	RMSE	sMAPE	MRAE	MASE	Average
Newmark (1965)	0.706	0.065	0.469	0.387	0.407
Makdisi and Seed (1978)	0.928	0.392	0.940	0.628	0.722
Hynes-Griffin and Franklin (1984)	0.000	0.000	0.000	0.000	0.000
Bray and Travasarou – 1 (2007)	0.179	0.285	0.145	0.072	0.170
Bray and Travasarou – 2 (2007)	0.508	0.608	0.572	0.442	0.533
Jibson 2 (2007)	0.359	0.093	0.236	0.173	0.215
Jibson 3 (2007)	0.404	0.094	0.433	0.370	0.325
Hsieh and Lee (2011)	0.860	0.180	0.589	0.461	0.522
Fotopoulou and Pitilakis – 1 (2015)	1.000	0.825	0.972	0.685	0.871
Fotopoulou and Pitilakis – 2 (2015)	0.828	0.994	0.962	0.759	0.886
Fotopoulou and Pitilakis – 3 (2015)	0.824	1.000	1.000	0.813	0.909
Fotopoulou and Pitilakis – 4 (2015)	0.030	0.877	0.971	1.000	0.719

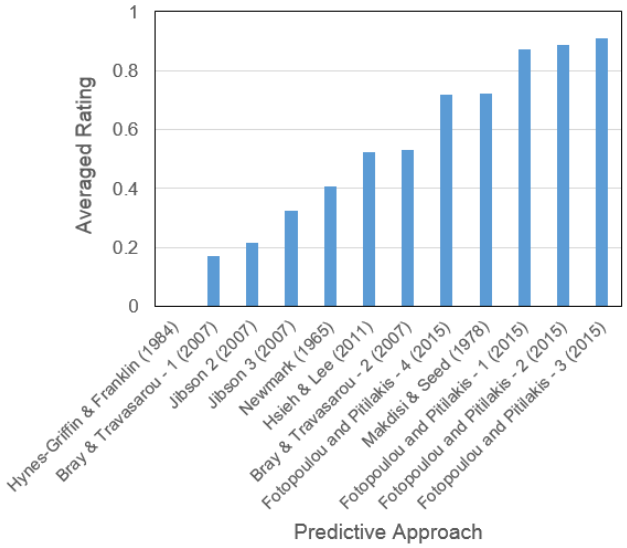

Figure 17. Averaged score of statistical measures for the empirical predictive approaches

4.4. Empirical predictive equations based on the Finite Element Method

A correlation analysis between the ground motion parameters and the horizontal seismic displacements calculated with the FEM model has been conducted. Initially, a regression analysis has been considered to address the engineering significance of negligible displacements (Bray and Travasarou (2007). A logistic regression using the probit fit model was performed to account for the probability of displacements greater than 0.1 cm. These regressions were also applied as weighting functions to find the most effective trend lines to estimate seismic displacements. After several regressions, it was possible to define the best and most adequate functional forms for the peak ground acceleration (PGA), Arias intensity (I_a), and the yield acceleration ratio (A_y/PGA).

Figure 18 illustrates the probability of non-zero displacements for PGA, Arias intensity, and the yield acceleration ratio. The functional form and coefficients of the probit models to compute the probability as a decimal number given a certain intensity measure (IM) are presented in Equation 27 and Table 7, respectively.

$$P(D > 0 \mid IM) = \frac{1}{[1 + a \cdot \exp(b \cdot (IM)^c)]^d} \qquad (27)$$

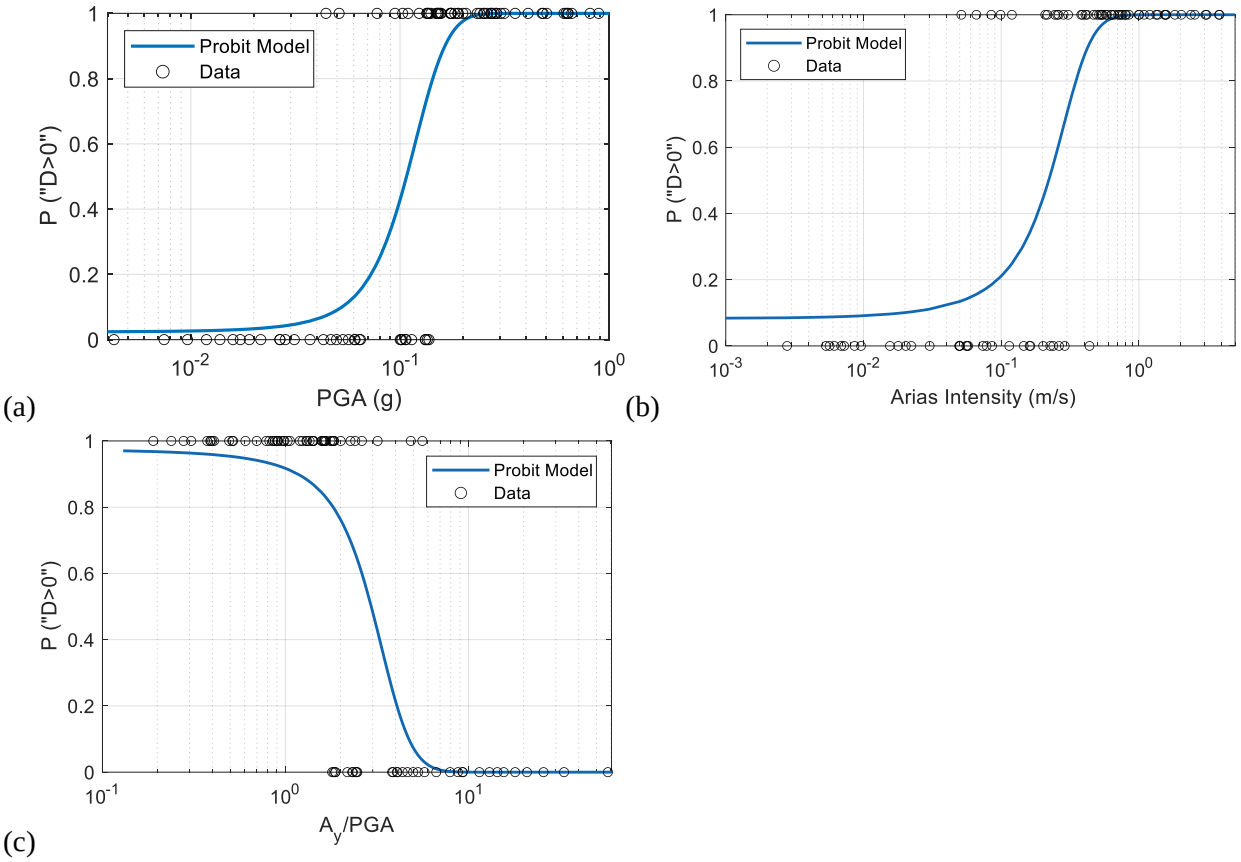

Figure 18. Probit regression for (a) PGA, (b) Arias intensity, and (c) A_y/PGA for the probability to obtain 'displacements greater than 0' (0.1 cm)

Table 7. Regression coefficients for estimating the probability of non-zero displacements given a certain intensity measure.

IM	**a**	**b**	**c**	**d**	R^2	RMSE
PGA (g)	1	-72.52	1.612	5.407	1	0.00239
I_a (m/s)	11.11	-10.87	1	1	0.9999	0.00476
A_y/PGA	0.0262	1.236	1	1	1	0

To account for the magnitude of non-zero displacement, Equations 28, 29, and 30 are proposed taking into account the IMs in scalar form. They are plotted in Figure 19 along with their predictive boundaries, data points, and their corresponding residuals (log D_{data} – log $D_{predicted}$). The equation forms have been selected among several regression analyses because of their highest goodness of fit. Table 8 shows the coefficients for the fitted line and the upper and lower predictive bounds with 95% confidence. It was not defined trend lines for PGV, PGD, $D_{5\text{-}95}$, and T_m because of their scattering. The data points of these IMs vs. FEM displacements are plotted in Figure 20.

$$\log(\text{D cm} \mid \text{IM}_1 = \text{PGA(g)}) = \frac{a \cdot \text{IM}_1 + b}{\text{IM}_1 + c} \qquad (28)$$

$$\log\left(\text{D cm} \mid \text{IM}_2 = I_a\left(\frac{m}{s}\right)\right) = a(\text{IM}_2)^b + c \qquad (29)$$

$$\log\left(\text{D cm} \mid \text{IM}_3 = \frac{A_y}{\text{PGA}}\right) = a \cdot \exp(-b \cdot \text{IM}_3) + c \qquad (30)$$

Table 8. Regression coefficients for estimating the non-zero displacements given a certain intensity measure. Scalar form.

IM	**a**	**b**	**c**	R^2	RMSE
PGA (g)	2.485 (1.77, 3.2)	-0.4178 (-0.5572, -0.2784)	0.1617 (-0.01231, 0.3357)	0.7562	0.3719
I_a (m/s)	84.08 (-936.6, 1105)	0.007486 (-0.08328, 0.09825)	-83.38 (-1104, 937.3)	0.9685	0.1331
A_y/PGA	3.662 (3.045, 4.278)	0.8873 (0.3878, 1.387)	-1.008 (-1.823, -0.1924)	0.7607	0.374

Similarly, a predictive equation is presented using the aforementioned intensity measures in a vectorial form as follow:

$$\log\left(\text{D cm}\middle|\ \text{IM}_1 = \text{PGA(g)},\ \text{IM}_2 = I_a\left(\frac{m}{s}\right),\ \text{IM}_3 = \frac{A_y}{\text{PGA}}\right) = a + b \cdot \text{IM}_1 + c \cdot \text{IM}_2 + d \cdot \text{IM}_3 \qquad (31)$$

Table 9. Regression coefficients for estimating nonzero displacements. Vectorial form.

a	**b**	**c**	**d**	R^2	Error Variance
0.37483	0.79333	0.15321	-0.33662	0.7591	0.18069

The predictive equations shall estimate seismic displacements for configurations similar to the present study that overall could be represented by its fundamental period, T_s = 0.18 s, and yield coefficient, k_y = 0.248, and for intensity measures values within the limits of the dataset. For different values, it can be stated that the more rigid the slope (lower fundamental periods), and the more dynamic strength (greater k_y), the smaller displacements the proposed models would predict compared to the actual ones (see Table 10). For a different combination of the T_s and k_y, the

predictive models could yield greater or smaller displacements and therefore should not be relied on. In Appendix F, the fitted functions are plotted along with the empirical data points.

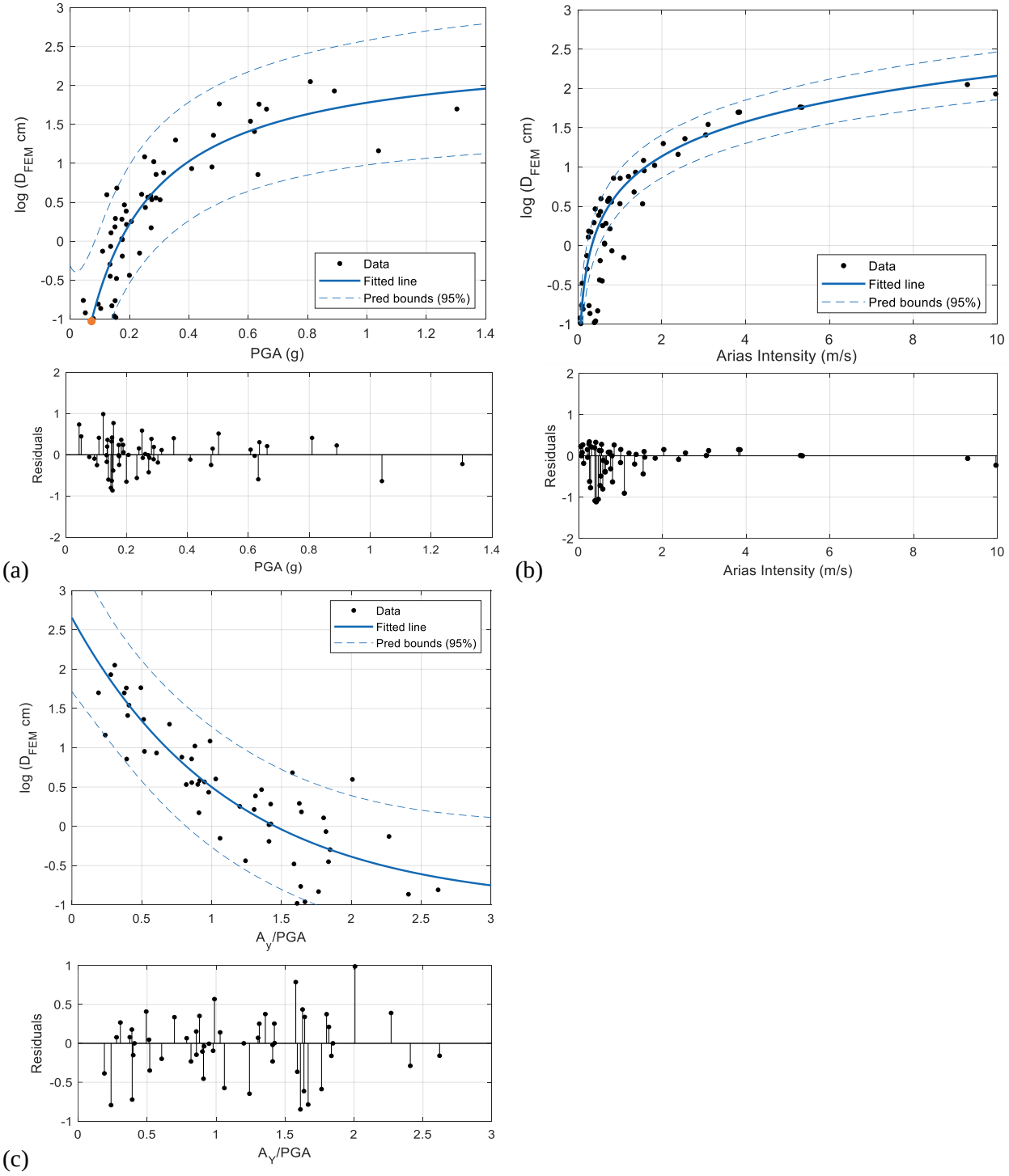

Figure 19. Regression of the horizontal seismic displacements versus intensity measures and their corresponding residuals (log D_{data} – log $D_{predicted}$) for: (a) PGA, (b) I_a, (c) A_y/PGA

In Figure 19a, it can be observed that for Equation 28, there is a truncated initial displacement of 0.1 cm for PGA's less than 0.0735 g, and in general, there is a high dispersion for PGA's greater than 0.4 g (e.g., predictive boundaries in the range of 2 cm to 100 cm for 0.4g). Similarly, in Figure 19b, for an Arias intensity equal to 4 m/s (Equation 29), the logarithmic predictive bounds vary approximately from 1.25 to 1.75 (i.e., about a half of a logarithmic scale), and this range increases for larger values of Arias intensity.

Table 10. Expected displacements for different fundamental periods and dynamic strength

T_s	$k_y = A_y/g$	FEM predictive equation yields…than real
<0.182 s (more Rigid)	>0.248 (more strength)	Smaller Displacements (not conservative)
>0.182 s (more flexible)	<0.248 (less strength)	Greater Displacements (conservative)

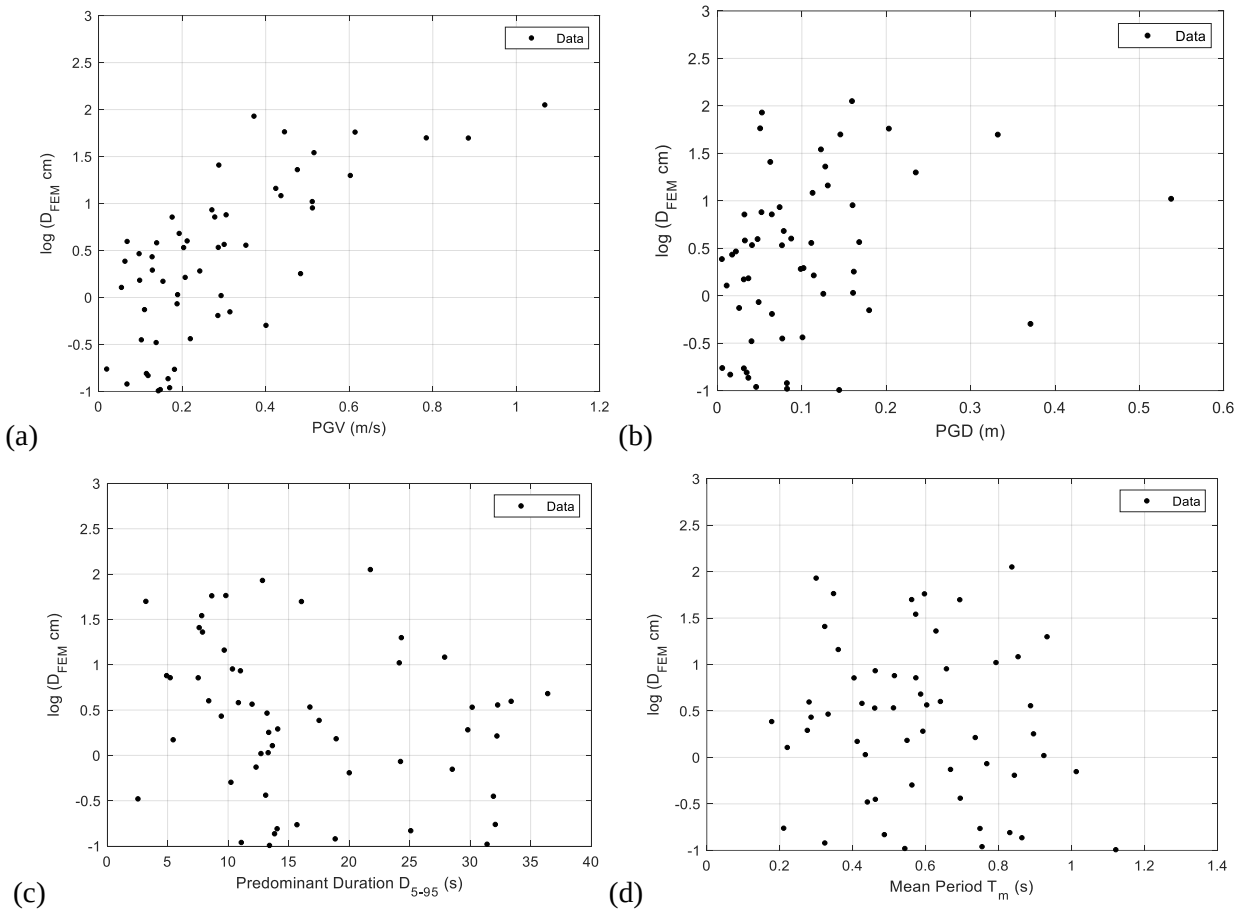

Figure 20. Seismic horizontal displacements versus intensity measures for: (a) PGV, (b) PGD, (c) D5-95, and (d) T_m

4.5. Effects of FEM mesh size on the predictive equations

As explained in section 2, the element size of the FEM computational mesh was selected to optimize the computational time, while targeting a maximum amount of frequency content of the input ground motions. To see the effects of finer element size in the horizontal displacements and the proposed predictive equations, one numerical model with finer element sizes varying from 0.14 m to 0.69 m, and an average of 0.357 m has been run with 10 different input motions. The records were selected so that they can cover the entire range of values of the ground motion parameters (PGA, I_a, A_y/PGA). The output numerical displacements are presented in Figure 21 along with the initial fitted line and predictive boundaries, and summarized in Table 11.

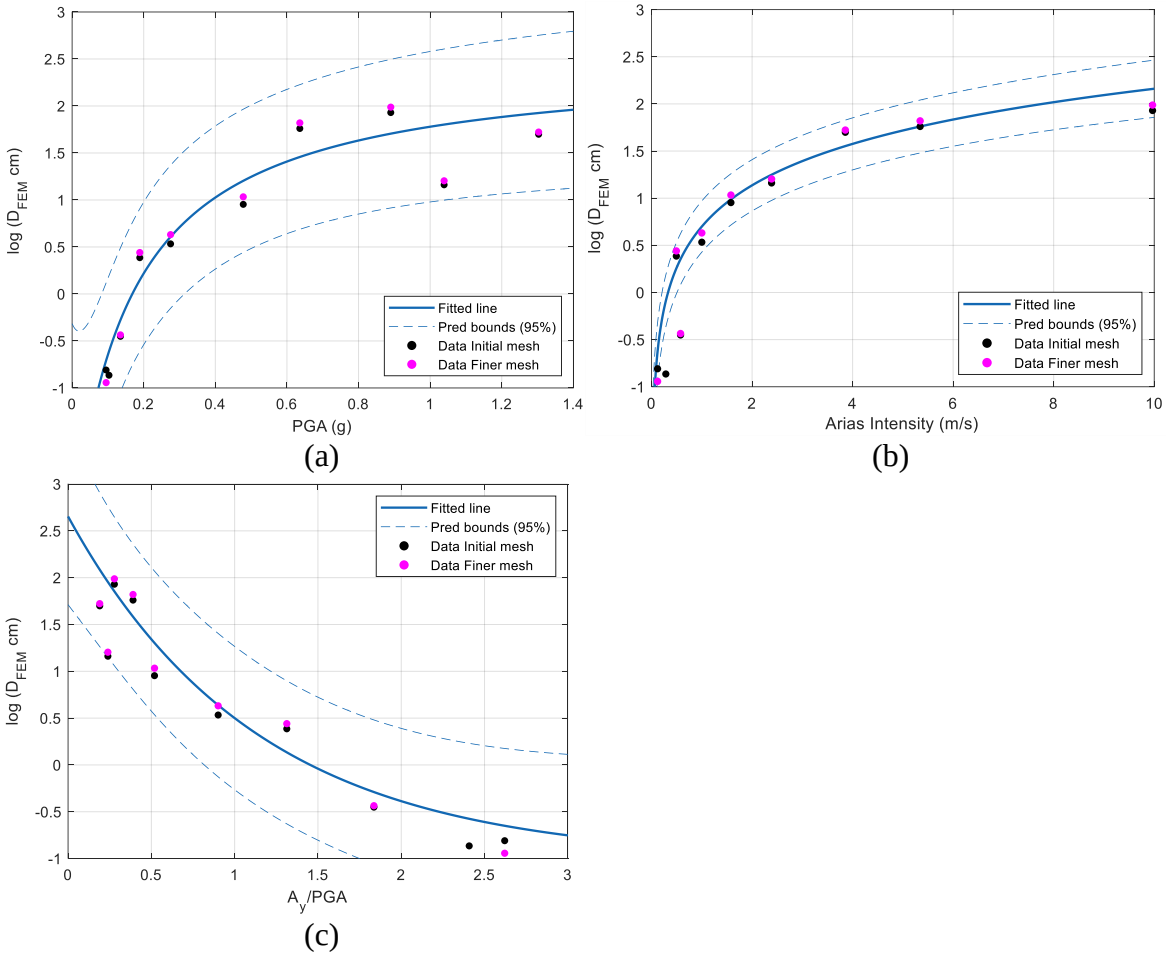

Figure 21. Log of displacement versus intensity measures. Data of finer mesh plotted on initial fitted line. (a) PGA, (b) Arias intensity, and (c) A_y/PGA

Table 11. Displacements for initial and finer mesh

Record	Intensity Measure			Log (D cm)		D (cm)	
	PGA (g)	I_a (m/s)	A_y/PGA	Initial	Finer	Initial	Finer
2	1.303	3.855	0.19	1.699	1.723	50.01	52.8
22	0.636	5.343	0.39	1.760	1.820	57.6	66.1
33	0.1350	0.5770	1.836	-0.451	-0.439	0.354	0.364
42	0.095	0.12	2.621	-0.809	-0.943	0.155	0.114
59	0.2750	1.00	0.9010	0.533	0.631	3.414	4.280
70	0.103	0.284	2.408	-0.865	-1.176	0.137	0.067
73	1.039	2.388	0.239	1.161	1.204	14.5	16
79	0.89	9.967	0.278	1.930	1.988	85.1	97.2
82	0.478	1.579	0.519	0.953	1.033	8.983	10.8
83	0.189	0.493	1.313	0.386	0.441	2.432	2.76

Overall, the displacements obtained with the finer mesh are slightly larger than the displacements obtained with the original mesh, but reasonably acceptable. Table 12 shows the R^2 and RMSE values obtained for the 10 data points considering the functional forms regressed in the previous section. Small absolute differences between the initial and finer fit measures can be observed; consequently, the mesh adopted initially considerably optimized the computation time for the 88 records without adverse effects.

Table 12. Absolute difference between initial and finer mesh fit measures

IM	Initial Mesh		Finer Mesh		Absolute difference	
	R^2	RMSE	R^2	RMSE	R^2	RMSE
PGA	0.9170	0.2887	0.9051	0.3353	0.0119	0.0466
Ia	0.8596	0.3755	0.8306	0.4488	0.029	0.0733
Ay/PGA	0.8858	0.3386	0.8817	0.3745	0.0041	0.0359

CHAPTER 5. CONCLUSIONS

In this study, the most renowned methods for slope stability analysis subjected to seismic loads were explained, including how these methodologies evaluate the onset of failure (stability analysis), and their applicability to predict post-failure deformations and final run-outs (post-failure analysis). These methods can be classified into three groups. The first approach is the pseudostatic analysis where the dynamic load is introduced as a single horizontal force through the application of the seismic coefficient k_s. Then, conventional limit equilibrium methods are performed to find a factor of safety. This approach does not provide any information for post-failure analysis. Another methodology is the sliding-block analysis which involves a double-integration of the ground accelerations that surpass the yield acceleration (A_y) in an acceleration time record until the relative velocity of the sliding mass is zero to find permanent displacements. The stability analysis is based upon allowable permanent displacements, and the post-failure analysis is restricted to small displacements (generally less than 1 m). There are different types of Newmark methods. The rigid approach considers the destabilized sliding mass as a rigid block while the decoupled and coupled methods take into account the deformability of the slope. The third method is the stress-deformation analysis, which consists of the application of numerical techniques (e.g. FEM) with sophisticated constitutive models. The stability analysis can be based on the estimation of the strength reduction factor (SRF), which resembles a factor of safety, or the evaluation of final deformations. The post-failure analysis, including large deformations, could be performed with particle-based numerical methods (e.g. MPM, SPH). Several empirical predictive equations were developed by different authors using the Newmark approach and numerical methods to estimate seismically induced displacements (resulting from 'slides' type of movements). The predicted displacements can be compared to allowable displacements to evaluate the performance of the slope.

Then, a comparison study of seismically induced displacements was carried out between 12 different empirical methods and the results of a FEM numerical model implemented in the Plaxis2D program. The geometry of a scale shaking-table experiment, validated with laboratory and published data (Hiraoka et al., 2013; and Bhandari et al., 2016), was scaled up by a factor of λ=10 to a prototype scale model to employ empirical predictive methods. The material properties were selected to preserve static slope stability and to maintain the factor of safety similar to the

scale model. The avoidance of this latest adjustment would cause the failure of the slope by self-weight. The selected empirical methods consisted of approaches developed by Newmark (1965), Makdisi and Seed (1978), Hynes-Griffin and Franklin (1984), Bray and Travasarou (2007), Jibson (2007), Hsieh and Lee (2011), and Fotopoulou and Pitilakis (2015).

The maximum permanent displacement calculated from the empirical approaches varies from 12.65 cm to 286.53 cm corresponding to the Hynes-Griffin and Franklin (1984) and the Fotopoulou and Pitilakis – 4 (2015), respectively. The maximum horizontal displacement obtained from the FEM is 112.20 cm resulting from the input excitation N°28. By observing the cumulative distributions of the computed displacements, the results of the stress-strain numerical method follow a similar trend to all the Fotopoulou and Pitilakis (2015) methods for displacements D>1 cm and to the Makdisi and Seed (1978) for approximately D>5 cm. Furthermore, by comparing the displacements obtained from both approaches directly, it can be observed that the FEM results are in good agreement with the Makdisi and Seed (1978), the Bray and Travasarou – 2 (2007), and the Fotopoulou and Pitilakis 2 and 3 (2015) methods. Fotopoulou 1 and 4 (2015) mostly overpredicts the FEM results; and overall, the rest of the empirical approaches underpredict the FEM results. This is reflected by the statistical measures and their scoring procedure similar to Jafarzadeh et al. (2019) where the empirical approaches that score the highest resemble the numerical results. From this analysis, the top empirical methods are precisely the formulations of Fotopoulou and Pitilakis (2015), Makdisi and Seed (1978), and Bray and Travasarou – 2 (2007). This can be attributed to the resemblance between the formulations and the presented model. The Fotopoulou and Pitilakis (2015) and Makdisi and Seed (1978) relationships were developed considering the slope's deformability by performing the amplification response using mesh based numerical methods (FDM and FEM respectively). In addition, the Fotopoulou and Pitilakis (2015) relationships proposed in 'Method 2' and 'Method 3' are functions of the PGA and A_y/PGA, which correlate well with the FEM results presented in this study. Finally, the Bray and Travasarou – 2 (2007) is a relationship proposed for 'rigid' slopes, which is consistent with the low fundamental period of the prototype slope model.

Finally, from the correlation analysis between the ground motion parameters and the horizontal seismic displacements calculated from the FEM; it was possible to define functional forms for predicting the calculated displacements as a function of the peak ground acceleration (PGA), Arias

intensity (I_a), and the yield acceleration ratio (A_y/PGA). The regression analysis included weighting functions determined by a logistic regression using the probit fit model which accounted for the probability of displacements greater than 0.1 cm. Then, the fourth correlation to estimate displacements was presented incorporating the PGA, I_a, and A_y/PGA. These predictive equations shall be applied to configurations similar to the slope conditions present in this study (i.e., homogeneous slopes settled on rigid or bedrock underlying material), with fundamental period, T_s = 0.18 s, yield coefficient, k_y = 0.248, and for intensity measures within the limits of the dataset's values.

5.1 Future work

Scaling models is a challenging subject because it needs to take into consideration different effects. Kutter (1995) describes the particle size effects, strain effects, boundary effects, and time scale conflict as the main problems of scaling to a laboratory model. These difficulties were particularly faced in this study given that the soil strength properties needed to be adjusted in order to maintain static slope stability and avoid failure due to self-weight. In this sense, it is recommended to perform a study considering a scale model performed in a centrifuge shaking table since these tests take into account more comprehensively the scaling implications because they address the gravitational effects.

In addition, the implications of a parametric analysis for different rigidities (represented by the fundamental period (T_s), which depends on the slope's height (H) and shear wave velocity (V_{s30})), and for different strengths (represented by the yield acceleration (A_y), which is a function of the soil shear strength parameters (cohesion and friction angle)) would be significant to implement a joint empirical predictive model. The parametric analysis could also be extended for different constitutive models that more accurately represent the soil behavior under seismic loads.

Furthermore, the application of other numerical models, that could address large deformations in a combined framework, would be important for the post-failure analysis. In this study, a higher uncertainty in the predictive boundaries was observed for larger seismic displacements. Thus, comparing them with the results of particle-based methods is recommended.

REFERENCES

Bartlett, S. (2011). *General types of 2D seismic analysis*.

Bhandari, T., Hamad, F., Moormann, C., Sharma, K. G., and Westrich, B. (2016). "Numerical modelling of seismic slope failure using MPM." *Computers and Geotechnics*, *75*, 126–134. https://doi.org/10.1016/j.compgeo.2016.01.017

Bray, J. D. (2007). "Simplified seismic slope displacement procedures." In K. D. Pitilakis (Ed.), *Earthquake Geotechnical Engineering* (pp. 327–353). Springer, Dordrecht. https://doi.org/10.1007/978-1-4020-5893-6_14

Bray, J. D., and Travasarou, T. (2007). "Simplified procedure for estimating earthquake-induced deviatoric slope displacements." *Journal of Geotechnical and Geoenvironmental Engineering*, *133*(4), 381–392. https://doi.org/10.1061/(ASCE)1090-0241(2007)133:4(381)

Bray, J. D., and Travasarou, T. (2009). "Pseudostatic coefficient for use in simplified seismic slope stability evaluation." *Journal of Geotechnical and Geoenvironmental Engineering*, *135*(9), 1336–1340. https://doi.org/10.1061/(ASCE)GT.1943-5606.0000012

Duncan, J. M. (1996). "State of the art: Limit equilibrium and finite-element analysis of slopes." *Journal of Geotechnical and Geoenvironmental Engineering*, *122*(7), 577–596. https://doi.org/10.1061/(ASCE)1090-0241(1997)123:9(894)

Duncan, J. M., Wright, S. G., and Brandon, T. L. (2014). "Soil strength and slope stability" (Second Edition). New Jersey: John Wiley & Sons.

Finn, W. D. L. (2013). "Seismic slope stability." In *Geo-Congress 2013* (pp. 2262–2288). Reston, VA: American Society of Civil Engineers. https://doi.org/10.1061/9780784412787.224

Fotopoulou, S. D., and Pitilakis, K. D. (2015). « Predictive relationships for seismically induced slope displacements using numerical analysis results." *Bulletin of Earthquake Engineering*, *13*(11), 3207–3238. https://doi.org/10.1007/s10518-015-9768-4

Harp, E. L., Wilson, R. C., and Wieczorek, G. F. (1981). "Landslides from the February 4, 1976, Guatemala earthquake." *U.S. Geological Survey Professional Paper*, *1204 A*. https://doi.org/10.3133/pp1204A

Highland, L. M., and Bobrowsky, P. (2008). "The landslide Handbook - A guide to understanding landslides." *US Geological Survey Circular*, (1325), 1–147. https://doi.org/10.3133/cir1325

Hiraoka, N. (2013). “Seismic slope failure modelling using the mesh-free SPH method.” *International Journal of Geomate*, *5*(1), 660–665. https://doi.org/10.21660/2013.9.3318

Hsieh, S.-Y., and Lee, C.-T. (2011). “Empirical estimation of the Newmark displacement from the Arias intensity and critical acceleration.” *Engineering Geology*, *122*(1–2), 34–42. https://doi.org/10.1016/j.enggeo.2010.12.006

Hyndman, R. J., and Koehler, A. B. (2006). “Another look at measures of forecast accuracy.” *International Journal of Forecasting*, *22*(4), 679–688. https://doi.org/10.1016/j.ijforecast.2006.03.001

Hynes-Griffin, M. E., and Franklin, A. G. (1984). “Rationalizing the seismic coefficient method.” In *Technical Information Center US Army Corps of Engineers* (pp. 1–40).

Jafarzadeh, F., Farahi-Jahromi, H., and Rajabigol, M. (2019). “Applicability of rigid block based approaches in predicting sandy slope displacements by 1g shaking table tests.” *Soil Dynamics and Earthquake Engineering*, *126*(September 2017), 105576. https://doi.org/10.1016/j.soildyn.2019.02.020

Jibson, R. W. (1993). “Predicting earthquake-induced landslide displacements using Newmark’s sliding block analysis.” *Transportation Research Record*, (8), 9–17.

Jibson, R. W. (2007). “Regression models for estimating coseismic landslide displacement.” *Engineering Geology*, *91*(2–4), 209–218. https://doi.org/10.1016/j.enggeo.2007.01.013

Jibson, R. W. (2010). “Methods for assessing the stability of slopes during earthquakes—A retrospective.” *Engineering Geology*, *122*(1–2), 43–50. https://doi.org/10.1016/j.enggeo.2010.09.017

Keefer, D. K. (2002). “Investigating landslides caused by earthquakes - A historical review.” *Surveys in Geophysics*, *23*(6), 473–510. https://doi.org/https://doi.org/10.1023/A:1021274710840

Khosravi, M., Leshchinsky, D., Meehan, C. L., and Khosravi, A. (2013). “Stability analysis of seismically loaded slopes using finite element techniques.” In *Geo-Congress 2013* (pp. 1310–1319). Reston, VA: American Society of Civil Engineers. https://doi.org/10.1061/9780784412787.132

Kieffer, D. S., Jibson, R., Rathje, E. M., and Kelson, K. (2006). “Landslides triggered by the 2004 Niigata Ken Chuetsu, Japan, Earthquake.” *Earthquake Spectra*, *22*(1_suppl), 47–73. https://doi.org/10.1193/1.2173021

Kramer, S. L. (2007). “Geotechnical earthquake engineering.” Pearson India

Kutter, B. L. (1995). “Recent Advances in centrifuge modeling of seismic shaking.” *International Conference on Recent Advances in Geotechnical Earthquake Engineering and Soil Dynamics.*, *4*, 927–941. Retrieved from https://scholarsmine.mst.edu/icrageesd/03icrageesd/session16/4/

Makdisi, F. I., and Seed, H. B. (1978). “Simplified procedure for estimating dam and embankment earthquake-induced deformations.” In *Journal of Geotechnical and Geoenvironmental Engineering*. American Society of Civil Engineers. Retrieved from https://trid.trb.org/view/74397

Meehan, C. L., and Vahedifard, F. (2013). “Evaluation of simplified methods for predicting earthquake-induced slope displacements in earth dams and embankments.” *Engineering Geology*, *152*(1), 180–193. https://doi.org/10.1016/j.enggeo.2012.10.016

Melo, C., and Sharma, S. (2004). “Seismic coefficients for pseudostatic slope analysis.” *13th World Conference on Earthquake Engineering*, (369), 15.

Newmark, N. M. (1965). “Effects of earthquakes on dams and embankments.” *Géotechnique*, *15*(2), 139–160. https://doi.org/10.1680/geot.1965.15.2.139

Plaxis. (2020). *PLAXIS 2D Reference manual*.

Plaxis. (2020). *PLAXIS Material Models*. *Plaxis Handbook 2D*.

Seed, H. B. (1979). “Considerations in the earthquake-resistant design of earth and rockfill dams.” *Géotechnique*, *29*(3), 215–263. https://doi.org/10.1680/geot.1979.29.3.215

Terzaghi, K. (1950). “Mechanism of landslides.” In *Application of Geology to Engineering Practice* (pp. 83–123). New York, N. Y.: Geological Society of America. https://doi.org/10.1130/Berkey.1950.83

Yerro, A., Alonso, E. E., and Pinyol, N. M. (2016). “Run-out of landslides in brittle soils.” *Computers and Geotechnics*, *80*, 427–439. https://doi.org/10.1016/j.compgeo.2016.03.001

Zabala, F., Rodari, R., and Oldecop, L. (2007). “Seismic analysis of geotechnical structures using the material point method.” *4th International Conference on Earthquake Geotechnical Engineering*, (1255).

APPENDIX A. Seismic records used for the numerical and empirical analysis

ID Record	Record Sequence Number	Earthquake Name	Year	Station Name	Magnitude	Mechanism	Rjb (km)	Rrup (km)	Vs30 (m/sec)	Lowest Useable Frequency (Hz)
1	1	"Helena_Montana-01"	1935	"Carroll College"	6	strike slip	2.07	2.86	593.35	0.1625
2	2	"Helena_Montana-02"	1935	"Helena Fed Bldg"	6	strike slip	2.09	2.92	551.82	0.5
3	28	"Parkfield"	1966	"Cholame - Shandon Array #12"	6.19	strike slip	17.64	17.64	408.93	0.125
4	33	"Parkfield"	1966	"Temblor pre-1969"	6.19	strike slip	15.96	15.96	527.92	0.1875
5	231	"Mammoth Lakes-01"	1980	"Long Valley Dam (Upr L Abut)"	6.06	Normal Oblique	12.56	15.46	537.16	0.1375
6	265	"Victoria_Mexico"	1980	"Cerro Prieto"	6.33	strike slip	13.8	14.37	471.53	0.375
7	297	"Irpinia_Italy-02"	1980	"Bisaccia"	6.2	Normal	14.73	14.74	496.46	0.1625
8	300	"Irpinia_Italy-02"	1980	"Calitri"	6.2	Normal	8.81	8.83	455.93	0.375
9	448	"Morgan Hill"	1984	"Anderson Dam (Downstream)"	6.19	strike slip	3.22	3.26	488.77	0.1625
10	451	"Morgan Hill"	1984	"Coyote Lake Dam - Southwest Abutment"	6.19	strike slip	0.18	0.53	561.43	0.125
11	295	"Irpinia_Italy-02"	1980	"Auletta"	6.2	Normal	28.69	29.86	476.62	0.15
12	299	"Irpinia_Italy-02"	1980	"Brienza"	6.2	Normal	41.73	42.65	561.04	0.35
13	325	"Coalinga-01"	1983	"Parkfield - Cholame 2E"	6.36	Reverse	41.99	42.92	522.74	0.1625
14	351	"Coalinga-01"	1983	"Parkfield - Gold Hill 3E"	6.36	Reverse	28.72	30.07	450.61	0.25
15	353	"Coalinga-01"	1983	"Parkfield - Gold Hill 4W"	6.36	Reverse	40.13	41.1	421.2	0.1625
16	17	"Southern Calif"	1952	"San Luis Obispo"	6	strike slip	73.35	73.41	493.5	0.1375
17	525	"N. Palm Springs"	1986	"Lake Mathews Dike Toe"	6.06	Reverse Oblique	66.59	66.71	592.42	1.25
18	528	"N. Palm Springs"	1986	"Murrieta Hot Springs"	6.06	Reverse Oblique	54.67	54.82	532.85	0.625
19	531	"N. Palm Springs"	1986	"Puerta La Cruz"	6.06	Reverse Oblique	67.38	67.5	442.7	0.625
20	539	"N. Palm Springs"	1986	"Temecula - 6th & Mercedes"	6.06	Reverse Oblique	64.68	64.8	416.15	0.25
21	557	"Chalfant Valley-02"	1986	"Tinemaha Res. Free Field"	6.19	strike slip	50.92	51.98	467.62	0.2875
22	820	"Georgia_USSR"	1991	"Zemi"	6.2	Reverse	51.33	51.38	432.58	0.15
23	913	"Big Bear-01"	1992	"LA - Temple & Hope"	6.46	strike slip	121.75	121.82	452.15	0.16
24	2491	"Chi-Chi_Taiwan-03"	1999	"CHY075"	6.2	Reverse	127.43	127.61	465.86	0.05
25	2546	"Chi-Chi_Taiwan-03"	1999	"HWA045"	6.2	Reverse	100.04	100.41	484.45	0.1
26	2558	"Chi-Chi_Taiwan-03"	1999	"ILA007"	6.2	Reverse	127.25	127.54	496.27	0.05
27	2563	"Chi-Chi_Taiwan-03"	1999	"ILA062"	6.2	Reverse	114.27	114.6	447.51	0.0875
28	2564	"Chi-Chi_Taiwan-03"	1999	"ILA064"	6.2	Reverse	113.72	114.05	488.61	0.0625
29	2569	"Chi-Chi_Taiwan-03"	1999	"KAU012"	6.2	Reverse	106.87	107.08	516.18	0.045
30	2570	"Chi-Chi_Taiwan-03"	1999	"KAU018"	6.2	Reverse	101.93	102.15	538.69	0.08
31	2581	"Chi-Chi_Taiwan-03"	1999	"KAU078"	6.2	Reverse	117.72	117.91	531.85	0.09
32	125	"Friuli_Italy-01"	1976	"Tolmezzo"	6.5	Reverse	14.97	15.82	505.23	0.1625
33	284	"Irpinia_Italy-01"	1980	"Auletta"	6.9	Normal	9.52	9.55	476.62	0.5
34	587	"New Zealand-02"	1987	"Matahina Dam"	6.6	Normal	16.09	16.09	551.3	0.25
35	753	"Loma Prieta"	1989	"Corralitos"	6.93	Reverse Oblique	0.16	3.85	462.24	0.1875
36	81	"San Fernando"	1971	"Pearblossom Pump"	6.61	Reverse	35.54	38.97	529.09	0.25
37	121	"Friuli_Italy-01"	1976	"Barcis"	6.5	Reverse	49.13	49.38	496.46	0.15
38	58	"San Fernando"	1971	"Cedar Springs Pumphouse"	6.61	Reverse	92.25	92.59	477.22	0.125
39	83	"San Fernando"	1971	"Puddingstone Dam (Abutment)"	6.61	Reverse	52.64	52.64	421.44	0.25
40	293	"Irpinia_Italy-01"	1980	"Torre Del Greco"	6.9	Normal	59.63	59.63	593.35	0.375
41	734	"Loma Prieta"	1989	"APEEL 3E Hayward CSUH"	6.93	Reverse Oblique	52.39	52.53	517.06	0.125
42	40	"Borrego Mtn"	1968	"San Onofre - So Cal Edison"	6.63	strike slip	129.11	129.11	442.88	0.1625
43	67	"San Fernando"	1971	"Isabella Dam (Aux Abut)"	6.61	Reverse	130	130.98	591	0.125
44	85	"San Fernando"	1971	"San Juan Capistrano"	6.61	Reverse	108.01	108.01	459.37	0.25

ID Record	Record Sequence Number	Earthquake Name	Year	Station Name	Magnitude	Mechanism	Rjb (km)	Rrup (km)	Vs30 (m/sec)	Lowest Useable Frequency (Hz)
45	825	"Cape Mendocino"	1992	"Cape Mendocino"	7.01	Reverse	0	6.96	567.78	0.07
46	1611	"Duzce_ Turkey"	1999	"Lamont 1058"	7.14	strike slip	0.21	0.21	529.18	0.075
47	830	"Cape Mendocino"	1992	"Shelter Cove Airport"	7.01	Reverse	26.51	28.78	518.98	0.5
48	3745	"Cape Mendocino"	1992	"Butler Valley Station 2"	7.01	Reverse	43.82	45.43	525.26	0.25
49	3750	"Cape Mendocino"	1992	"Loleta Fire Station"	7.01	Reverse	23.46	25.91	515.65	0.0625
50	3751	"Cape Mendocino"	1992	"South Bay Union School"	7.01	Reverse	33.23	35.22	459.04	0.1875
51	3759	"Landers"	1992	"Whitewater Trout Farm"	7.28	strike slip	27.05	27.05	425.02	0.375
52	14	"Kern County"	1952	"Santa Barbara Courthouse"	7.36	Reverse	81.3	82.19	514.99	0.375
53	886	"Landers"	1992	"Puerta La Cruz"	7.28	strike slip	94.48	94.48	442.7	0.3
54	1627	"Caldiran_ Turkey"	1976	"Maku"	7.21	strike slip	50.78	50.82	432.58	0
55	1770	"Hector Mine"	1999	"Big Bear Lake - Fire Station"	7.13	strike slip	61.85	61.85	406.7	0.026
56	1782	"Hector Mine"	1999	"Forest Falls Post Office"	7.13	strike slip	74.92	74.92	436.14	0
57	1831	"Hector Mine"	1999	"San Jacinto - Soboba"	7.13	strike slip	92.71	92.71	447.22	0.03
58	1832	"Hector Mine"	1999	"Seven Oaks Dam Project Office"	7.13	strike slip	87.2	87.2	564.93	0.039
59	1833	"Hector Mine"	1999	"Snow Creek"	7.13	strike slip	72.88	72.88	523.59	0.065
60	1838	"Hector Mine"	1999	"Whitewater Trout Farm"	7.13	strike slip	62.91	62.91	425.02	0.13
61	4453	"Montenegro_ Yugoslavia"	1979	"Dubrovnik - Pomorska Skola"	7.1	Reverse	65.88	66.67	585.04	1.25
62	13	"Kern County"	1952	"Pasadena - CIT Athenaeum"	7.36	Reverse	122.65	125.59	415.13	0.25
63	837	"Landers"	1992	"Baldwin Park - N Holly"	7.28	strike slip	131.92	131.92	544.68	0.06
64	846	"Landers"	1992	"Chatsworth - Devonshire"	7.28	strike slip	172.45	172.45	409.4	0.05
65	852	"Landers"	1992	"Duarte - Mel Canyon Rd."	7.28	strike slip	126.33	126.33	459.14	0.07
66	875	"Landers"	1992	"La Crescenta - New York"	7.28	strike slip	148.47	148.47	411.55	0.1
67	1197	"Chi-Chi_ Taiwan"	1999	"CHY028"	7.62	Reverse Oblique	3.12	3.12	542.61	0.15
68	1208	"Chi-Chi_ Taiwan"	1999	"CHY046"	7.62	Reverse Oblique	24.1	24.1	442.15	0.05
69	1230	"Chi-Chi_ Taiwan"	1999	"CHY079"	7.62	Reverse Oblique	46.59	47.52	573.04	0.0375
70	1248	"Chi-Chi_ Taiwan"	1999	"CHY109"	7.62	Reverse Oblique	40.37	41.03	573.04	0.25
71	1249	"Chi-Chi_ Taiwan"	1999	"CHY110"	7.62	Reverse Oblique	40.37	41.03	573.04	0.25
72	1164	"Kocaeli_ Turkey"	1999	"Istanbul"	7.51	strike slip	49.66	51.95	595.2	0.0875
73	1169	"Kocaeli_ Turkey"	1999	"Maslak"	7.51	strike slip	52.96	55.3	445.66	0.1125
74	1190	"Chi-Chi_ Taiwan"	1999	"CHY019"	7.62	Reverse Oblique	49.98	50.53	497.53	0.0375
75	1191	"Chi-Chi_ Taiwan"	1999	"CHY022"	7.62	Reverse Oblique	63.21	64.15	564.07	0.0375
76	1214	"Chi-Chi_ Taiwan"	1999	"CHY057"	7.62	Reverse Oblique	56.67	56.93	411.46	0.0375
77	1218	"Chi-Chi_ Taiwan"	1999	"CHY061"	7.62	Reverse Oblique	57.5	58.75	538.69	0.0875
78	1263	"Chi-Chi_ Taiwan"	1999	"HWA012"	7.62	Reverse Oblique	53	56.65	414.42	0.15
79	1266	"Chi-Chi_ Taiwan"	1999	"HWA015"	7.62	Reverse Oblique	47.04	51.12	453.05	0.025
80	1267	"Chi-Chi_ Taiwan"	1999	"HWA016"	7.62	Reverse Oblique	48.19	52.18	576.55	0.0625
81	1268	"Chi-Chi_ Taiwan"	1999	"HWA017"	7.62	Reverse Oblique	47.04	51.11	578.11	0.025
82	1151	"Kocaeli_ Turkey"	1999	"Balikesir"	7.51	strike slip	180.24	180.24	468.44	0.0375
83	1159	"Kocaeli_ Turkey"	1999	"Eregli"	7.51	strike slip	141.37	142.29	585.09	0.0625
84	1370	"Chi-Chi_ Taiwan"	1999	"KAU040"	7.62	Reverse Oblique	140.09	141.51	567.64	0.05
85	1372	"Chi-Chi_ Taiwan"	1999	"KAU043"	7.62	Reverse Oblique	170.99	172.16	538.49	0.025
86	1379	"Chi-Chi_ Taiwan"	1999	"KAU052"	7.62	Reverse Oblique	167.9	169.09	573.04	0.0375
87	1381	"Chi-Chi_ Taiwan"	1999	"KAU057"	7.62	Reverse Oblique	112.48	113.54	535.13	0.0375
88	1394	"Chi-Chi_ Taiwan"	1999	"KAU082"	7.62	Reverse Oblique	168.72	169.9	573.04	0.025

APPENDIX B. Histograms of Intensity Measures

(a) Moment Magnitude, (b) Shear Velocity Vs_{30}, (c) Arias intensity, (d) Rupture Distance

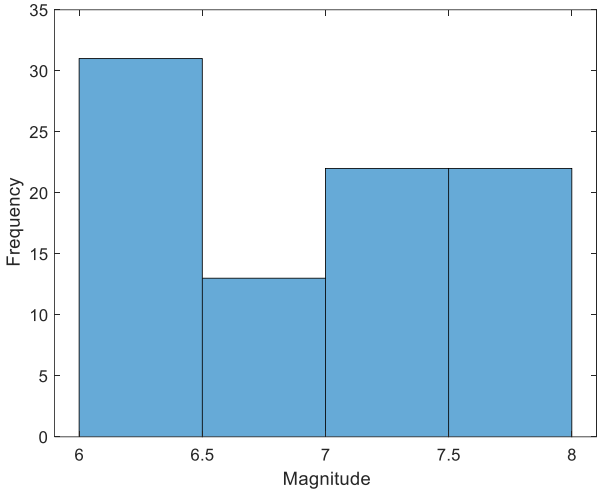

(a)

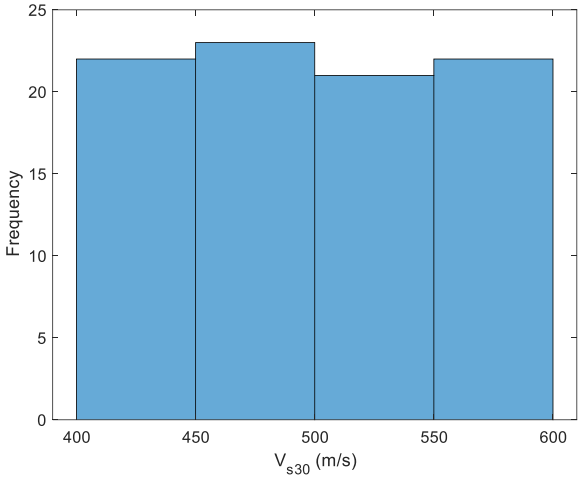

(b)

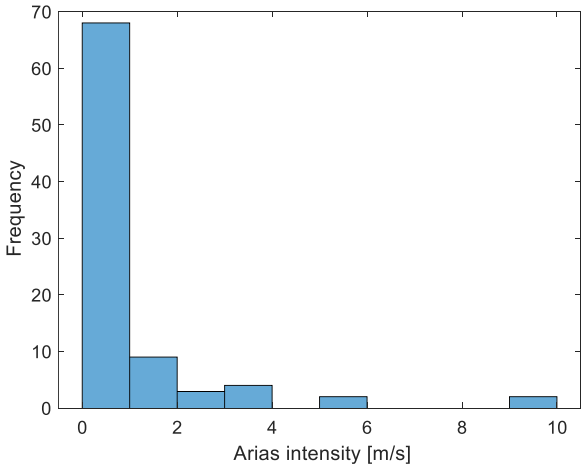

(c)

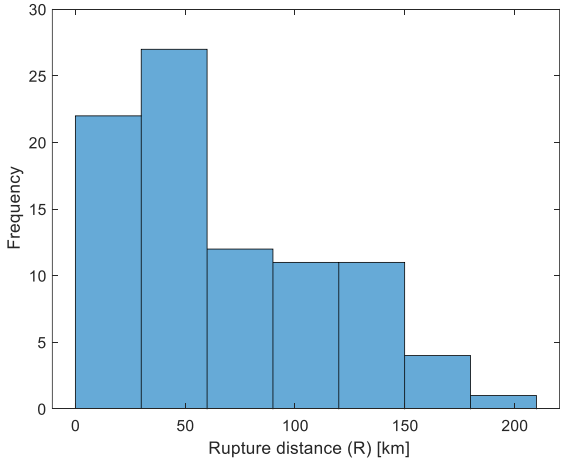

(d)

APPENDIX C. Correlations between ground motion parameters

(a) PGA vs Magnitude, (b) Rupture Distance vs Magnitude, (c) Arias intensity vs PGA, (d) PGV vs PGA, (e) Mean Period vs PGA, (f) Predominant Duration vs PGA

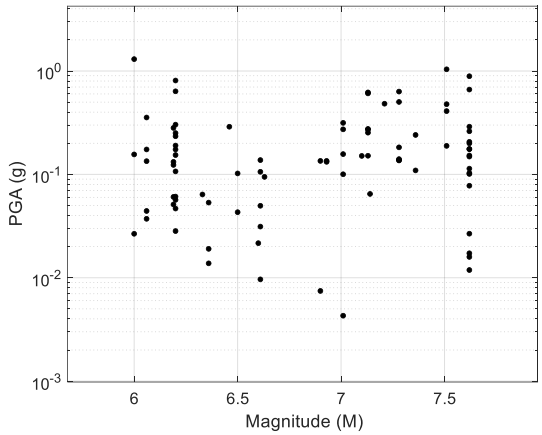

(a)

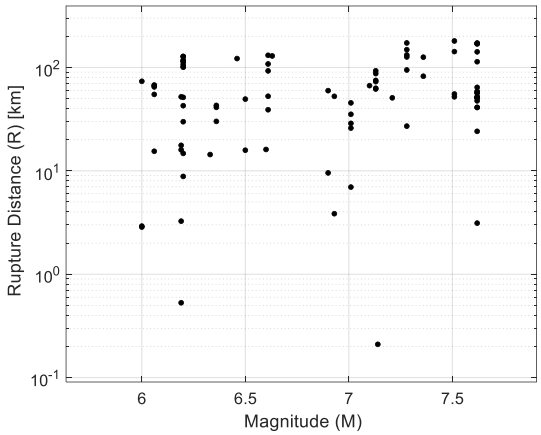

(b)

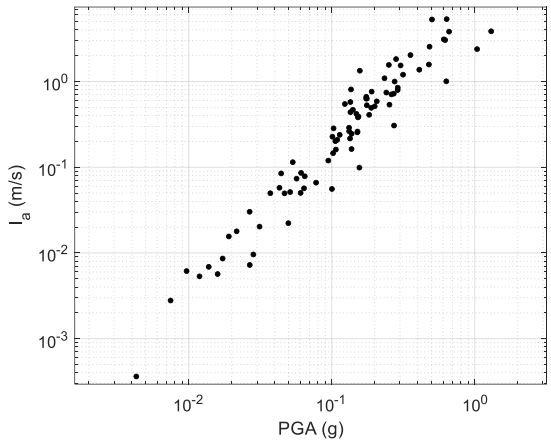

(c)

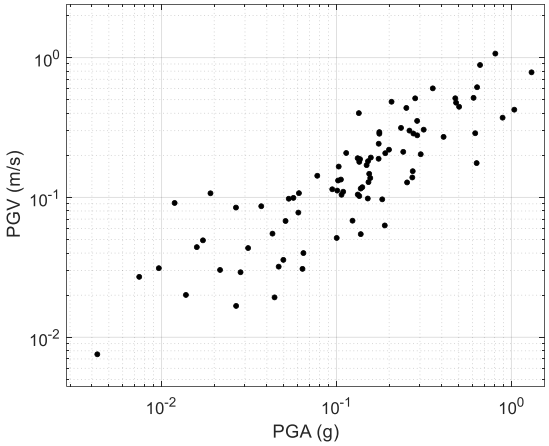

(d)

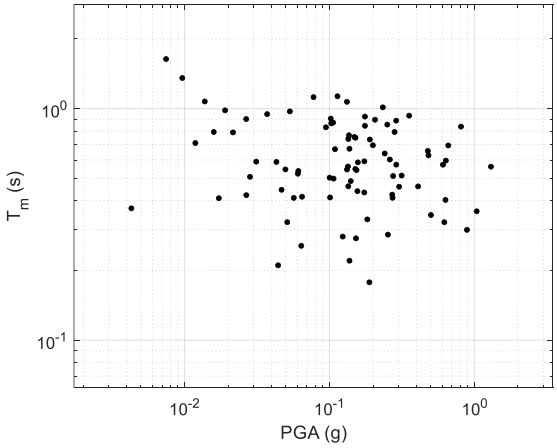

(e)

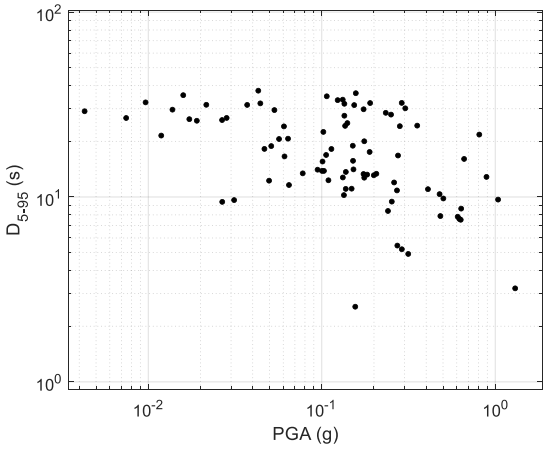

(f)

APPENDIX D. Summary of seismic displacements and ground motion parameters

ID Record	PGA [g]	PGV [m/s]	PGD [m]	Ia [m/s]	T_m [s]	$D_{5\text{-}95}$ [s]	A_v/PGA	Newmark (1965) [cm]	Makdisi and Seed (1978) [cm]	Hynes-Griffin and Franklin (1984) [cm]	Bray and Travasarou – 1 (2007) [cm]	Bray and Travasarou – 2 (2007) [cm]	Jibson – 2 (2007) [cm]	Jibson – 3 (2007) [cm]	Hsieh and Lee (2011) [cm]	Fotopoulou and Pitilakis – 1 (2015) [cm]	Fotopoulou and Pitilakis – 2 (2015) [cm]	Fotopoulou and Pitilakis – 3 (2015) [cm]	Fotopoulou and Pitilakis – 4 (2015) [cm]	FEM [cm]
1	0.156	0.138	0.040	0.099	0.440	2.550	1.589	0.00000	0.00000	0.00000	0.00008	0.10837	0.00029	0.00155	0.00052	0.92044	0.48025	0.46073	0.98207	0.33150
2	1.303	0.784	0.146	3.855	0.561	3.205	0.190	6.04711	14.51933	0.12654	1.49935	29.36094	1.92923	41.40028	4.57510	23.96020	43.85935	45.61082	54.17965	50.01000
3	0.124	0.068	0.047	0.547	0.280	33.390	2.007	0.00000	0.00000	0.00000	0.00179	0.05392	0.01773	0.00166	0.03604	0.26116	0.32345	0.31459	0.28813	3.95000
4	0.132	0.191	0.055	0.290	1.070	33.600	1.877	0.00000	0.00000	0.00000	0.00146	0.06712	0.00386	0.00150	0.00745	1.79358	0.37322	0.36393	1.87964	0.08970
5	0.044	0.019	0.006	0.085	0.211	32.080	5.601	0.00000	0.00000	0.00000	0.00000	0.00140	0.00020	0.00001	0.00035	0.02360	0.03401	0.03133	0.02466	0.17310
6	0.064	0.031	0.007	0.057	0.256	20.670	3.878	0.00000	0.00000	0.00000	0.00000	0.00585	0.00008	0.00004	0.00013	0.06163	0.08590	0.08285	0.05916	0.08200
7	0.174	0.189	0.161	0.632	0.434	13.310	1.424	0.00000	0.19797	0.00000	0.00898	0.16142	0.02515	0.00669	0.05171	1.76907	0.67471	0.66564	1.97966	1.07200
8	0.061	0.107	0.139	0.086	0.538	16.570	4.064	0.00000	0.00000	0.00000	0.00230	0.00476	0.00021	0.00004	0.00037	0.61205	0.07252	0.06875	0.61400	0.06320
9	0.061	0.078	0.096	0.050	0.523	24.085	4.095	0.00000	0.00000	0.00000	0.00524	0.00462	0.00006	0.00003	0.00010	0.33534	0.07098	0.06719	0.33501	0.09590
10	0.051	0.068	0.082	0.051	0.323	18.850	4.846	0.00000	0.00000	0.00000	0.00003	0.00250	0.00006	0.00001	0.00010	0.25866	0.04962	0.04667	0.25846	0.12000
11	0.028	0.029	0.032	0.010	0.507	26.760	8.763	0.00000	0.00000	0.00000	0.00002	0.00026	0.00000	0.00000	0.00000	0.05338	0.01415	0.01303	0.05274	0.04000
12	0.057	0.099	0.100	0.074	0.412	20.585	4.370	0.00000	0.00000	0.00000	0.00098	0.00366	0.00014	0.00003	0.00025	0.52934	0.06216	0.05876	0.52973	0.05100
13	0.053	0.098	0.022	0.115	0.973	29.510	4.647	0.00000	0.00000	0.00000	0.00071	0.00305	0.00042	0.00003	0.00075	0.54059	0.05940	0.05710	0.52028	0.05930
14	0.014	0.020	0.008	0.007	1.074	29.670	17.984	0.00000	0.00000	0.00000	0.00016	0.00001	0.00000	0.00000	0.00000	0.02781	0.00334	0.00305	0.02619	0.01550
15	0.019	0.107	0.102	0.016	0.983	25.840	13.017	0.00000	0.00000	0.00000	0.00007	0.00005	0.00000	0.00000	0.00001	0.63881	0.00664	0.00614	0.60277	0.04900
16	0.027	0.085	0.064	0.030	0.901	26.065	9.308	0.00000	0.00000	0.00000	0.00324	0.00019	0.00002	0.00000	0.00003	0.37004	0.01118	0.01003	0.38942	0.03580
17	0.037	0.086	0.037	0.050	0.947	31.475	6.670	0.00000	0.00000	0.00000	0.00082	0.00072	0.00006	0.00000	0.00009	0.39235	0.02346	0.02146	0.40724	0.02140
18	0.134	0.401	0.371	0.216	0.562	10.235	1.847	0.00000	0.00000	0.00000	0.02628	0.06811	0.00192	0.00135	0.00362	6.92913	0.35999	0.34585	7.43595	0.50500
19	0.355	0.603	0.235	2.034	0.933	24.316	0.698	0.12547	7.14331	0.00041	1.33838	1.25328	0.41569	0.19812	0.93725	14.87798	2.85125	2.84240	22.96486	19.89800
20	0.174	0.242	0.099	0.665	0.592	29.808	1.423	0.00000	0.98717	0.00000	0.09100	0.15584	0.02834	0.00691	0.05849	2.69878	0.62762	0.60898	3.16773	1.91500
21	0.282	0.511	0.538	1.827	0.793	24.145	0.880	0.00000	2.50983	0.00002	0.36775	0.67828	0.32147	0.07692	0.71872	11.37005	1.86943	1.87613	16.20663	10.50000
22	0.636	0.614	0.203	5.343	0.597	8.650	0.390	12.86424	19.03328	0.01968	1.45129	5.98818	4.22463	3.18920	10.28022	16.05958	10.63172	11.01843	46.10032	57.60000
23	0.289	0.353	0.111	0.797	0.887	32.275	0.858	0.00000	2.56905	0.00003	0.39275	0.78661	0.04381	0.05325	0.09173	6.13645	2.28053	2.36573	6.57256	3.60000
24	0.251	0.436	0.113	1.564	0.853	27.895	0.988	0.00000	4.54181	0.00000	3.78656	0.48555	0.22109	0.04512	0.48824	8.47786	1.46745	1.46796	11.42932	12.13000
25	0.303	0.204	0.076	1.541	0.460	30.170	0.818	0.06132	6.49965	0.00006	0.02101	0.83645	0.21336	0.09230	0.47061	2.03149	2.19303	2.20960	2.72614	3.40000
26	0.234	0.314	0.180	1.092	1.013	28.525	1.060	0.00000	0.60963	0.00000	0.92149	0.39488	0.09330	0.02818	0.20026	4.58330	1.26379	1.26086	5.62230	0.70340
27	0.047	0.032	0.003	0.050	0.446	18.200	5.306	0.00000	0.00000	0.00000	0.01692	0.00179	0.00006	0.00001	0.00009	0.06349	0.04113	0.03860	0.06323	0.01780
28	0.809	1.068	0.159	9.291	0.836	21.755	0.306	50.15911	18.26585	0.04517	15.44024	10.69275	15.95101	10.92907	40.54928	45.31403	17.72546	18.53872	286.52738	112.20000
29	0.190	0.207	0.114	0.763	0.736	32.215	1.304	0.00000	0.74477	0.00000	0.23365	0.21168	0.03942	0.01041	0.08226	2.09926	0.81347	0.80522	2.41111	1.63700
30	0.107	0.105	0.050	0.161	0.499	35.035	2.320	0.00000	0.00000	0.00000	0.00016	0.03350	0.00094	0.00048	0.00174	0.58310	0.23898	0.23144	0.59380	0.08770
31	0.154	0.148	0.082	0.390	0.543	31.400	1.611	0.00000	0.03029	0.00000	0.01341	0.10960	0.00789	0.00318	0.01560	1.11179	0.51880	0.50943	1.18529	0.10470
32	0.043	0.055	0.059	0.058	0.589	37.575	5.756	0.00000	0.00000	0.00000	0.00017	0.00143	0.00008	0.00001	0.00014	0.19199	0.04062	0.03938	0.17530	0.08000
33	0.135	0.102	0.077	0.577	0.462	31.925	1.836	0.00000	0.22376	0.00000	0.00651	0.08775	0.02015	0.00240	0.04112	0.68833	0.57162	0.60704	0.61960	0.35420
34	0.022	0.030	0.012	0.018	0.789	31.525	11.474	0.00000	0.00000	0.00000	0.00013	0.00010	0.00000	0.00000	0.00001	0.06450	0.00988	0.00944	0.05673	0.04680
35	0.135	0.180	0.073	0.438	0.740	27.516	1.837	0.00000	0.00000	0.00000	0.22013	0.08841	0.01042	0.00206	0.02081	1.99310	0.58057	0.61874	1.72973	0.08310
36	0.106	0.134	0.232	0.202	0.871	16.875	2.339	0.00000	0.00000	0.00000	0.03095	0.03652	0.00162	0.00053	0.00304	1.05149	0.29241	0.29724	0.95657	0.06000
37	0.102	0.132	0.125	0.146	0.906	22.490	2.427	0.00000	0.00000	0.00000	0.10389	0.03130	0.00074	0.00038	0.00136	0.98792	0.25495	0.25544	0.91807	0.07600
38	0.031	0.043	0.025	0.020	0.590	9.620	7.933	0.00000	0.00000	0.00000	0.00001	0.00043	0.00001	0.00000	0.00001	0.12709	0.02178	0.02113	0.11149	0.04050
39	0.010	0.031	0.027	0.006	1.356	32.475	25.696	0.00000	0.00000	0.00000	0.00016	0.00000	0.00000	0.00000	0.00000	0.06830	0.00179	0.00166	0.05976	0.03900
40	0.007	0.027	0.027	0.003	1.637	26.740	33.248	0.00000	0.00000	0.00000	0.00004	0.00000	0.00000	0.00000	0.00000	0.05696	0.00121	0.00115	0.04571	0.02820
41	0.132	0.105	0.021	0.263	0.546	12.750	1.874	0.00000	0.00000	0.00000	0.00023	0.08279	0.00306	0.00143	0.00588	0.72806	0.55599	0.59208	0.61012	0.06170
42	0.095	0.114	0.035	0.120	0.830	14.050	2.621	0.00000	0.00000	0.00000	0.00059	0.02503	0.00046	0.00025	0.00083	0.78311	0.23212	0.23550	0.69669	0.15520
43	0.138	0.116	0.029	0.163	0.671	11.060	1.803	0.00000	0.00000	0.00000	0.00058	0.08584	0.00097	0.00127	0.00179	0.79577	0.50880	0.52235	0.71836	0.04700
44	0.050	0.036	0.009	0.022	0.546	12.250	4.988	0.00000	0.00000	0.00000	0.00023	0.00252	0.00001	0.00001	0.00001	0.08831	0.05842	0.05770	0.07750	0.00730
45	0.100	0.051	0.010	0.056	0.503	13.840	2.472	0.00000	0.00000	0.00000	0.00102	0.03389	0.00007	0.00021	0.00013	0.19531	0.32201	0.34257	0.15336	0.04390
46	0.065	0.040	0.006	0.078	0.416	11.606	3.831	0.00000	0.00000	0.00000	0.00000	0.00766	0.00017	0.00005	0.00029	0.12729	0.13600	0.14451	0.09663	0.01070
47	0.004	0.008	0.008	0.000	0.371	29.080	57.719	0.00000	0.00000	0.00000	0.00000	0.00000	0.00000	0.00000	0.00000	0.00540	0.00040	0.00037	0.00419	0.00480
48	0.273	0.154	0.031	0.307	0.412	5.460	0.909	0.02145	0.04109	0.00001	0.00048	0.77573	0.00442	0.02493	0.00859	1.52997	2.70482	2.98905	1.26317	1.48700

ID Record	PGA [g]	PGV [m/s]	PGD [m]	Ia [m/s]	T_m [s]	$D_{5\text{-}95}$ [s]	A_y/PGA	Newmark (1965) [cm]	Makdisi and Seed (1978) [cm]	Hynes-Griffin and Franklin (1984) [cm]	Bray and Travasarou Coupled (2007) [cm]	Bray and Travasarou Rigid (2007) [cm]	Jibson – 2 (2007) [cm]	Jibson – 3 (2007) [cm]	Hsieh and Lee (2011) [cm]	Fotopoulou and Pitilakis – 1 (2015) [cm]	Fotopoulou and Pitilakis – 2 (2015) [cm]	Fotopoulou and Pitilakis – 3 (2015) [cm]	Fotopoulou and Pitilakis – 4 (2015) [cm]	FEM [cm]
49	0.315	0.305	0.052	1.202	0.514	4.920	0.787	0.08860	14.64500	0.00010	0.04010	1.17072	0.11767	0.09338	0.25451	5.50825	3.67762	4.08645	5.43998	7.58480
50	0.157	0.193	0.079	1.338	0.586	36.410	1.578	0.00000	0.10473	0.00000	0.00341	0.14672	0.15204	0.00688	0.33164	2.33094	0.83683	0.90558	2.36526	4.80600
51	0.136	0.188	0.049	0.809	0.767	24.247	1.818	0.00000	0.21210	0.00000	0.47342	0.10070	0.04539	0.00301	0.09514	2.40157	0.71544	0.79521	2.02434	0.85660
52	0.241	0.212	0.087	0.744	0.640	8.400	1.030	0.00000	0.00000	0.00000	0.00010	0.59460	0.03716	0.02543	0.07739	3.08384	2.50243	2.86939	2.50622	4.00000
53	0.502	0.445	0.051	5.298	0.347	9.815	0.494	2.39856	36.21468	0.00618	0.56169	4.44430	4.14070	1.28155	10.06934	12.08492	11.45399	13.37775	25.00259	58.00000
54	0.483	0.476	0.128	2.551	0.628	7.885	0.513	3.52533	32.08758	0.00487	1.17831	3.93293	0.71608	0.73069	1.64367	13.41984	10.14203	11.72953	16.36226	22.94550
55	0.607	0.516	0.123	3.104	0.573	7.820	0.408	1.79978	19.93063	0.01617	2.45440	6.90868	1.14680	1.96724	2.67345	15.23579	15.83766	18.30217	21.24352	34.80000
56	0.621	0.288	0.063	3.049	0.323	7.610	0.399	0.89306	10.05677	0.01777	0.00266	7.29669	1.09848	2.11857	2.55718	5.11115	16.59490	19.19324	7.04838	25.68000
57	0.271	0.139	0.032	0.722	0.425	10.850	0.914	0.00318	5.09001	0.00001	0.00823	0.79024	0.03459	0.03954	0.07187	1.30683	2.85282	3.19732	1.13165	3.81910
58	0.253	0.128	0.017	0.537	0.286	9.440	0.979	0.00040	0.00000	0.00000	0.00000	0.64715	0.01702	0.02573	0.03455	1.12101	2.46451	2.75491	0.93554	2.71070
59	0.275	0.286	0.041	1.000	0.512	16.760	0.901	0.01916	0.17661	0.00001	0.00033	0.82270	0.07556	0.05007	0.16107	5.06803	2.93880	3.29544	4.63934	3.41400
60	0.151	0.182	0.031	0.261	0.749	15.690	1.637	0.00000	0.00000	0.00000	0.00017	0.13502	0.00301	0.00239	0.00576	2.15774	0.82511	0.90448	1.70390	0.17190
61	0.151	0.098	0.037	0.255	0.549	18.930	1.643	0.00000	0.00000	0.00000	0.00005	0.13250	0.00285	0.00233	0.00546	0.67684	0.80628	0.88058	0.53861	1.52590
62	0.109	0.110	0.026	0.209	0.668	12.310	2.269	0.00000	0.00000	0.00000	0.00223	0.04979	0.00176	0.00060	0.00332	0.90091	0.46599	0.51851	0.65787	0.74280
63	0.138	0.055	0.011	0.246	0.220	13.660	1.801	0.00000	0.00000	0.00000	0.00002	0.10372	0.00260	0.00160	0.00496	0.23781	0.72955	0.81118	0.17911	1.28000
64	0.183	0.097	0.022	0.409	0.332	13.215	1.357	0.00000	1.18580	0.00000	0.04596	0.25295	0.00886	0.00631	0.01759	0.69549	1.33211	1.49718	0.54126	2.92600
65	0.140	0.118	0.015	0.468	0.487	25.094	1.765	0.00000	0.00000	0.00000	1.01989	0.11078	0.01222	0.00249	0.02454	1.01104	0.76205	0.84798	0.79614	0.14760
66	0.633	0.176	0.032	1.006	0.403	7.530	0.392	0.05275	0.27766	0.01919	0.00027	7.96437	0.07662	1.22064	0.16341	2.12733	18.70322	22.03676	1.86527	7.17600
67	0.027	0.017	0.002	0.007	0.423	9.410	9.289	0.00000	0.00000	0.00000	0.00441	0.00030	0.00000	0.00000	0.00000	0.02874	0.02672	0.02907	0.01867	0.00260
68	0.012	0.091	0.134	0.005	0.710	21.485	20.869	0.00000	0.00000	0.00000	0.00000	0.00001	0.00000	0.00000	0.00000	0.68774	0.00478	0.00504	0.44656	0.05560
69	0.016	0.044	0.073	0.006	0.793	35.525	15.585	0.00000	0.00000	0.00000	0.00001	0.00004	0.00000	0.00000	0.00000	0.17612	0.00889	0.00948	0.11436	0.01000
70	0.103	0.166	0.037	0.284	0.864	13.840	2.408	0.00000	0.00000	0.00000	0.14140	0.04386	0.00369	0.00057	0.00712	2.11320	0.47184	0.54030	1.45088	0.13660
71	0.176	0.286	0.065	0.529	0.843	20.014	1.410	0.00000	0.00000	0.00000	1.05142	0.24698	0.01636	0.00629	0.03316	5.82041	1.47277	1.72111	4.19629	0.64270
72	0.409	0.271	0.074	1.373	0.462	11.020	0.606	0.56697	0.00000	0.00151	0.00006	2.76298	0.16189	0.27431	0.35386	5.11546	8.38423	9.98622	4.51080	8.57000
73	1.039	0.424	0.131	2.388	0.360	9.680	0.239	1.09382	0.00000	0.08379	0.00179	27.28052	0.61082	13.27538	1.39474	11.82538	60.75468	74.96939	12.77259	14.50000
74	0.114	0.208	0.123	0.239	1.130	18.180	2.181	0.00000	0.00000	0.00000	0.00018	0.06104	0.00243	0.00076	0.00463	3.21093	0.58256	0.66960	2.18468	0.00500
75	0.662	0.885	0.332	3.821	0.693	16.060	0.375	8.93159	29.19738	0.02296	0.00346	9.77772	1.88887	3.06625	4.47626	48.44595	24.68285	30.33467	67.47121	49.80000
76	0.078	0.143	0.144	0.066	1.121	13.420	3.192	0.00000	0.00000	0.00000	0.00873	0.01670	0.00011	0.00009	0.00019	1.59167	0.25922	0.29368	1.04614	0.10160
77	0.152	0.129	0.102	0.382	0.275	14.100	1.627	0.00000	0.00000	0.00000	0.00004	0.15773	0.00749	0.00303	0.01479	1.30721	1.08633	1.26262	0.91516	1.95670
78	0.101	0.112	0.077	0.227	0.413	15.550	2.454	0.00000	0.00000	0.00000	0.00009	0.04120	0.00216	0.00047	0.00409	1.00750	0.45355	0.51899	0.68389	0.08220
79	0.890	0.372	0.053	9.967	0.300	12.840	0.278	13.51957	30.46270	0.05861	0.00012	19.81746	18.87916	16.38422	48.25979	9.54810	46.41039	57.68437	45.45771	85.10000
80	0.206	0.483	0.162	0.587	0.895	13.355	1.201	0.00000	2.31409	0.00000	0.76386	0.40372	0.02103	0.01234	0.04299	15.60667	2.07251	2.43679	11.38382	1.79400
81	0.289	0.278	0.064	0.848	0.573	5.215	0.857	0.06196	5.19492	0.00003	0.11594	1.08970	0.05088	0.05539	0.10705	5.53772	4.25278	5.06492	4.25579	7.19500
82	0.478	0.512	0.160	1.579	0.657	10.360	0.519	3.20057	31.44027	0.00455	0.92281	4.15724	0.22631	0.53580	0.50015	16.81307	11.63957	13.94506	15.44808	8.98290
83	0.189	0.063	0.005	0.493	0.178	17.520	1.313	0.00000	0.00000	0.00000	0.00000	0.29833	0.01386	0.00795	0.02795	0.33272	1.61573	1.86867	0.24605	2.43200
84	0.017	0.049	0.064	0.009	0.410	26.350	14.375	0.00000	0.00000	0.00000	0.00000	0.00005	0.00000	0.00000	0.00000	0.21723	0.01056	0.01129	0.14114	0.04860
85	0.149	0.170	0.046	0.420	0.754	11.090	1.668	0.00000	0.42633	0.00000	0.08365	0.14591	0.00941	0.00291	0.01873	2.20623	1.03109	1.19729	1.55639	0.10950
86	0.176	0.293	0.125	0.634	0.924	12.715	1.410	0.00000	1.46100	0.00000	0.78657	0.24709	0.02532	0.00697	0.05208	6.11511	1.47322	1.72164	4.50278	1.04790
87	0.261	0.301	0.168	0.708	0.603	11.980	0.949	0.00000	1.21611	0.00001	0.27783	0.81184	0.03297	0.03383	0.06840	6.40523	3.42201	4.05970	4.78643	3.67300
88	0.200	0.220	0.101	0.514	0.695	13.105	1.242	0.00000	0.99055	0.00000	0.26101	0.36444	0.01527	0.01006	0.03088	3.55704	1.92878	2.26489	2.55682	0.36400
MAX	1.30	1.07	0.54	9.97	1.64	37.58	57.72	50.16	36.21	0.127	15.44	29.36	18.88	41.40	48.26	48.45	60.75	74.97	286.53	112.2
MIN	0.00	0.01	0.00	0.00	0.18	2.55	0.19	0.00	0.00	0.000	0.00	0.00	0.00	0.00	0.00	0.01	0.00	0.00	0.00	0.0026

APPENDIX E. Histograms of seismic displacements obtained from the empirical and numerical methods

(a) Newmark (1965), (b) Makdisi and Seed (1978), (c) Hynes-Griffin and Franklin (1984), (d) Bray and Travasarou – 1 (2007), (e) Bray and Travasarou – 2 (2007), (f) Jibson 2 (2007), (g) Jibson 3 (2007), (h) Hsieh and Lee (2011), (i) Fotopoulou and Pitilakis – 1 (2015), (j) Fotopoulou and Pitilakis – 2 (2015), (k) Fotopoulou and Pitilakis – 3 (2015), (l) Fotopoulou and Pitilakis – 4 (2015), (m) Finite Element Method

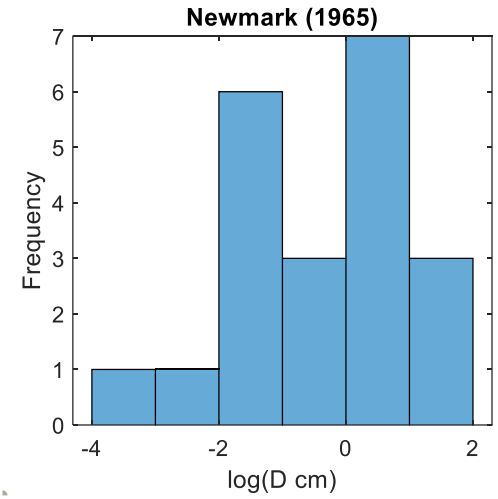

(a)

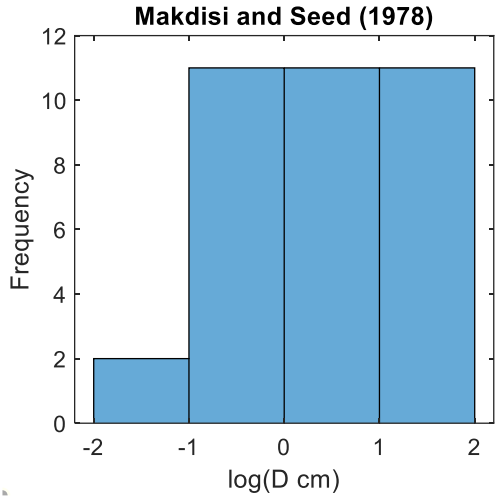

(b)

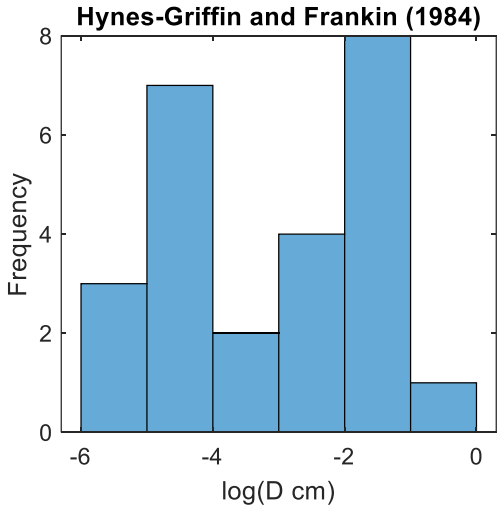

(c)

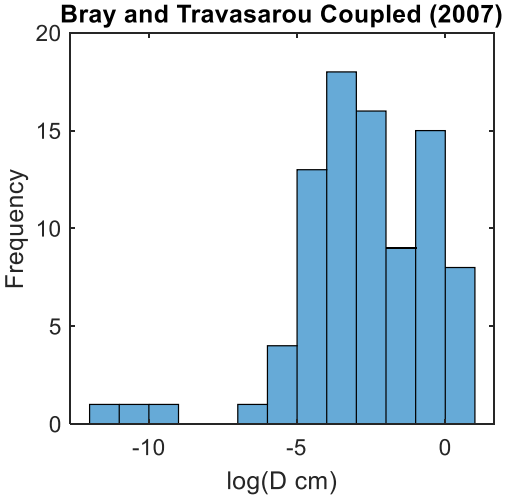

(d)

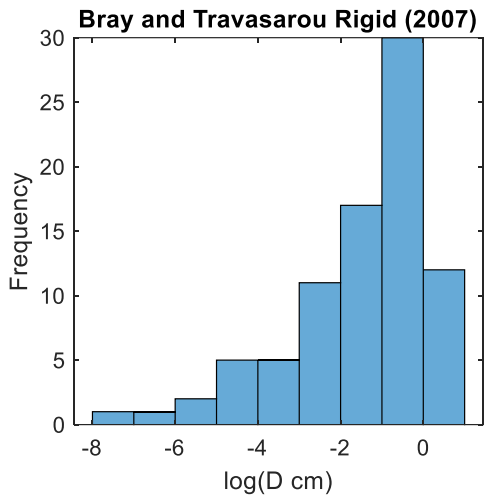
Bray and Travasarou Rigid (2007)
Frequency
log(D cm)

(e)

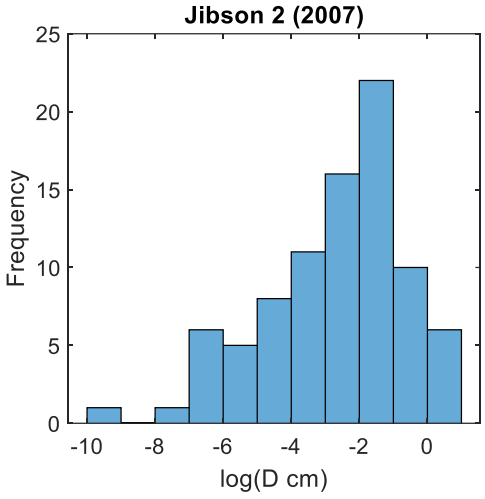
Jibson 2 (2007)
Frequency
log(D cm)

(f)

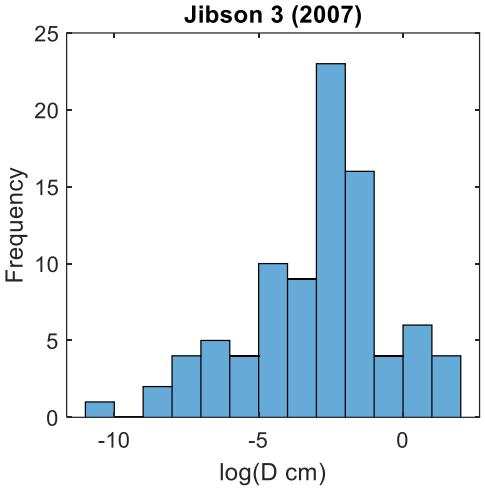
Jibson 3 (2007)
Frequency
log(D cm)

(g)

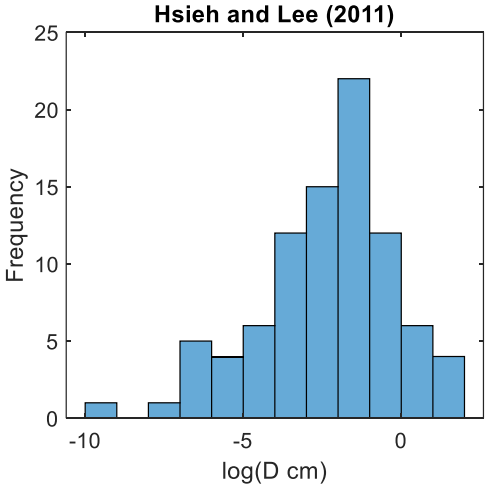
Hsieh and Lee (2011)
Frequency
log(D cm)

(h)

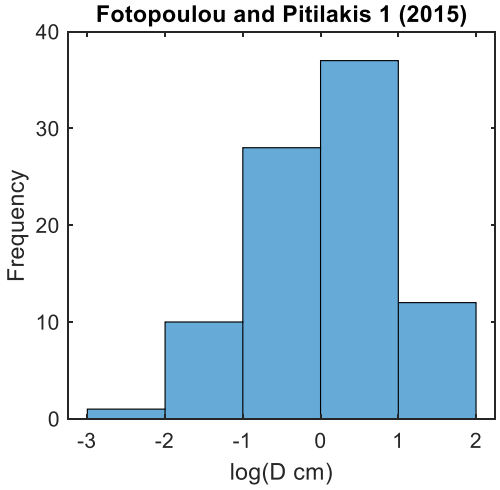
Fotopoulou and Pitilakis 1 (2015)
Frequency
log(D cm)

(i)

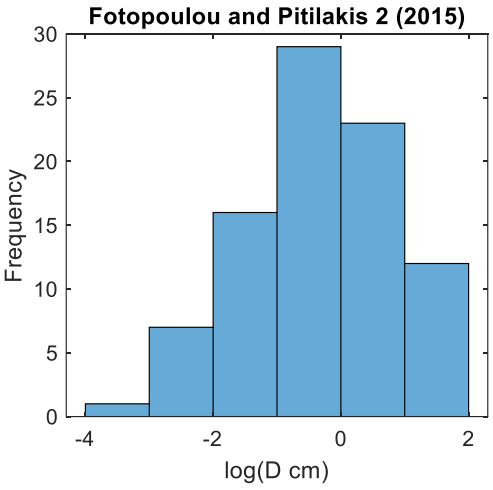
Fotopoulou and Pitilakis 2 (2015)
Frequency
log(D cm)

(j)

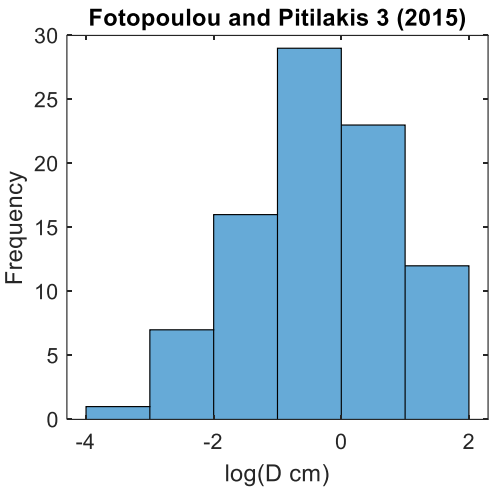
Fotopoulou and Pitilakis 3 (2015)
Frequency
log(D cm)

(k)

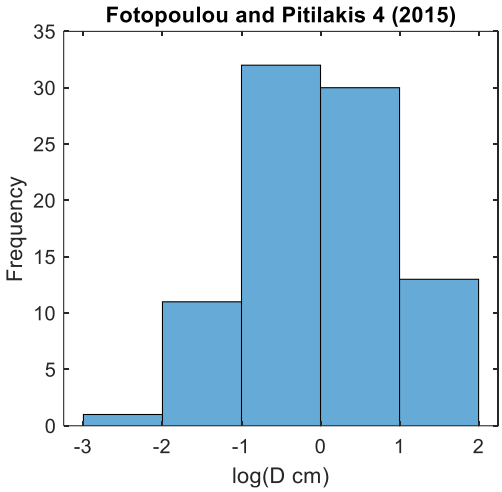
Fotopoulou and Pitilakis 4 (2015)
Frequency
log(D cm)

(l)

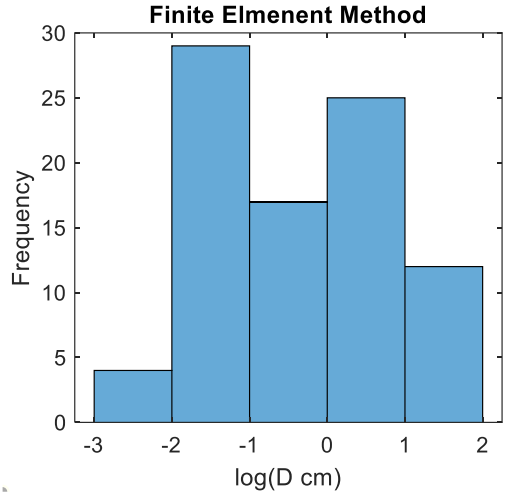
Finite Elmenent Method
Frequency
log(D cm)

(m)

APPENDIX F. Fitted functions with empirical data points

Peak Ground Acceleration versus log displacements for: (a) Fitted line (FEM), Newmark (1965), Makdisi and Seed (1978), Hynes-Griffin and Franklin (1984); (b) Fitted line (FEM), Bray and Travasarou – 1 (2007), Bray and Travasarou – 2 (2007), Jibson 2 (2007); (c) Fitted line (FEM), Jibson 3 (2007), Hsieh and Lee (2011), Fotopoulou and Pitilakis – 1 (2015); and (d) Fitted line (FEM), Fotopoulou and Pitilakis – 2,3,4 (2015)

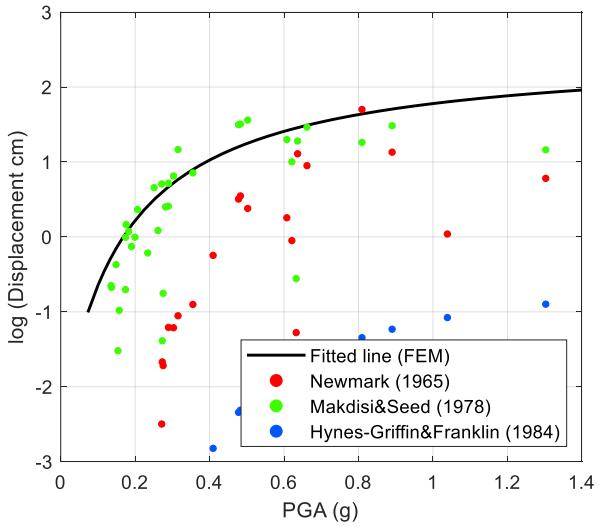

(a)

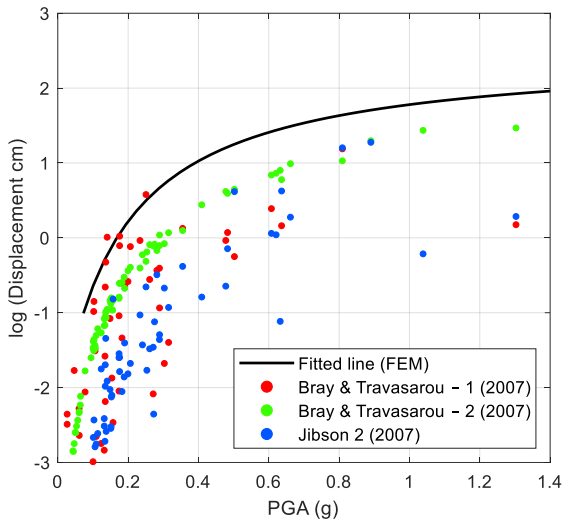

(b)

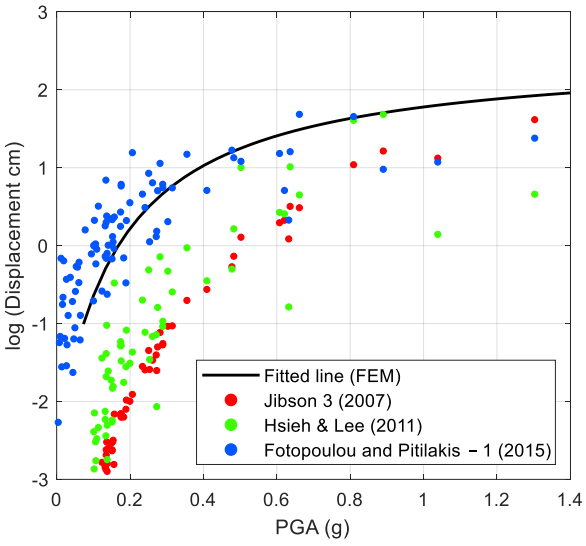

(c)

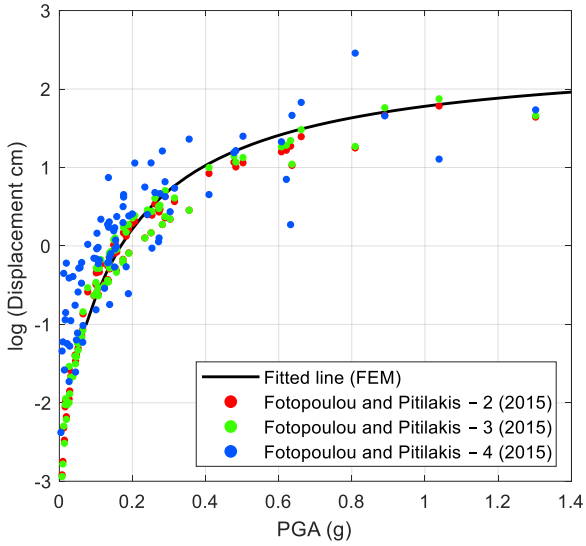

(d)

Arias intensity versus log displacements for: (a) Fitted line (FEM), Newmark (1965), Makdisi and Seed (1978), Hynes-Griffin and Franklin (1984); (b) Fitted line (FEM), Bray and Travasarou – 1 (2007), Bray and Travasarou – 2 (2007), Jibson 2 (2007); (c) Fitted line (FEM), Jibson 3 (2007), Hsieh and Lee (2011), Fotopoulou and Pitilakis – 1 (2015); and (d) Fitted line (FEM), Fotopoulou and Pitilakis – 2,3,4 (2015)

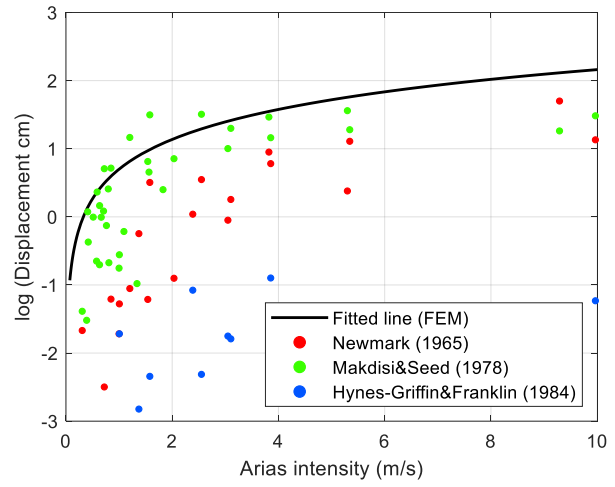

(a)

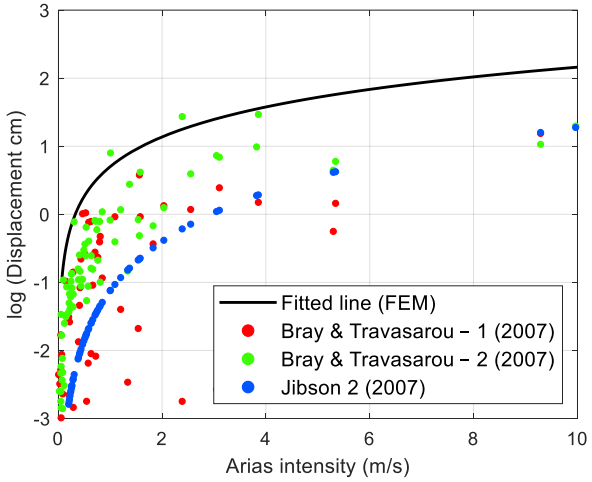

(b)

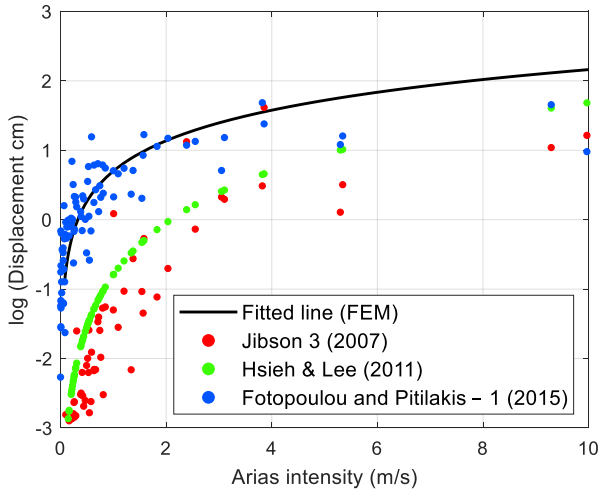

(c)

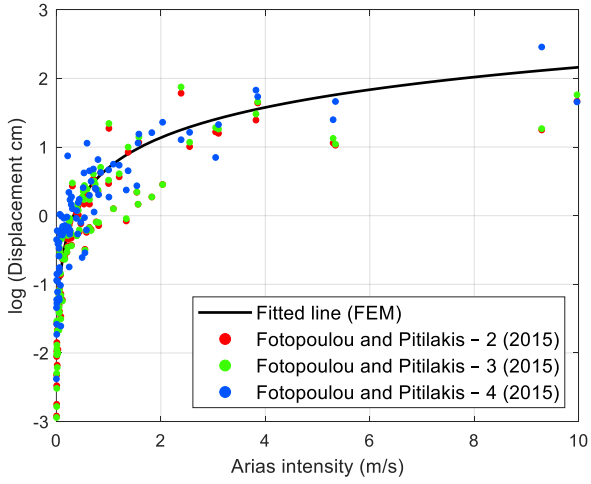

(d)

Yield acceleration ratio versus log displacements for: (a) Fitted line (FEM), Newmark (1965), Makdisi and Seed (1978), Hynes-Griffin and Franklin (1984); (b) Fitted line (FEM), Bray and Travasarou – 1 (2007), Bray and Travasarou – 2 (2007), Jibson 2 (2007); (c) Fitted line (FEM), Jibson 3 (2007), Hsieh and Lee (2011), Fotopoulou and Pitilakis – 1 (2015); and (d) Fitted line (FEM), Fotopoulou and Pitilakis – 2,3,4 (2015)

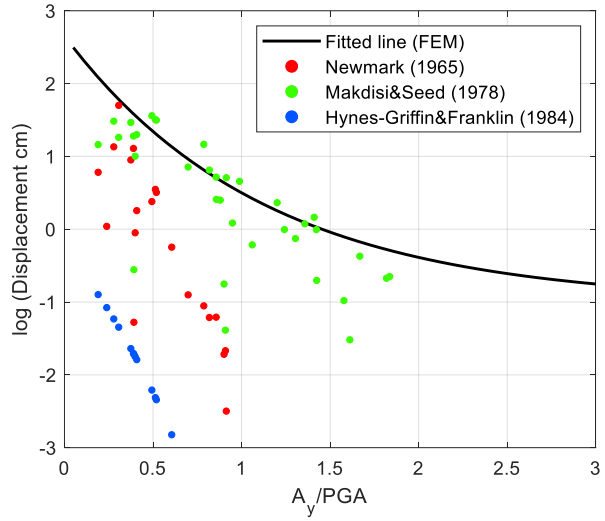

(a)

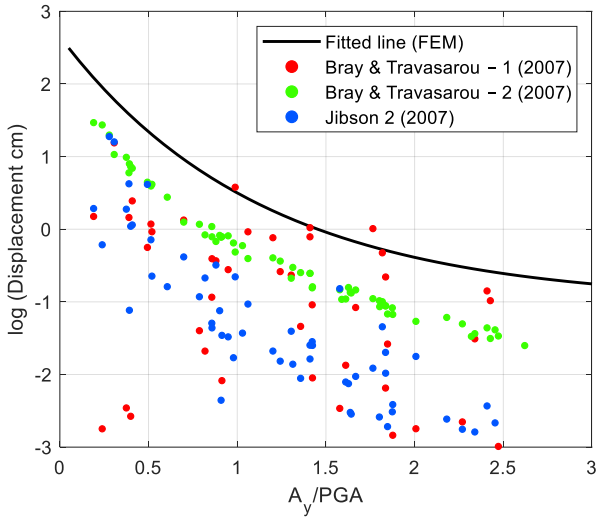

(b)

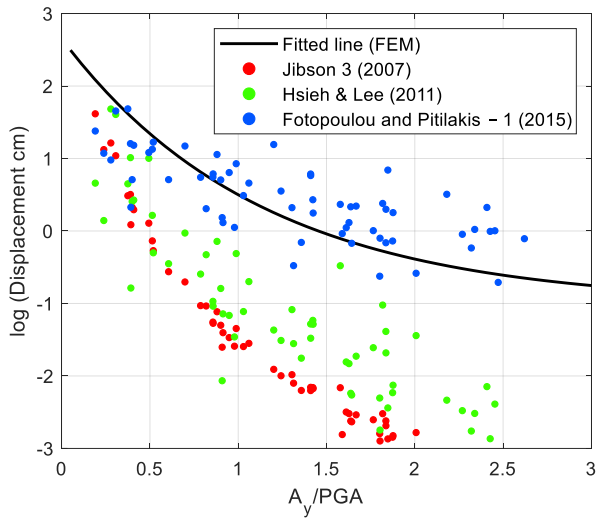

(c)

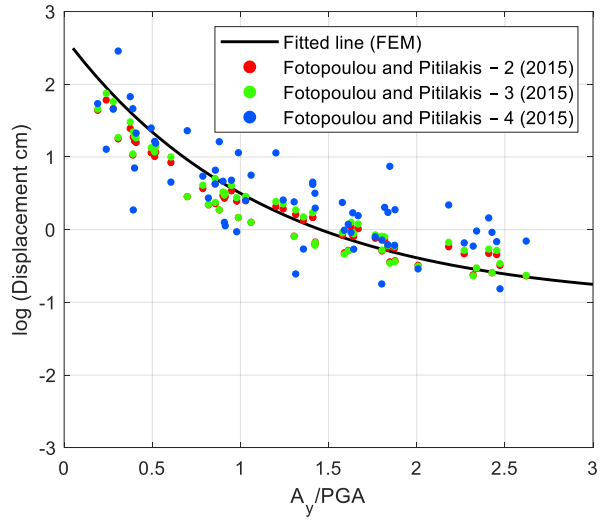

(d)